CFTP/11-015

A Common Framework for Dark Matter, Leptogenesis and Neutrino Masses

François-Xavier Josse-Michaux* and Emiliano Molinaro†
Centro de Física Teórica de Partículas (CFTP), Instituto Superior Técnico, Technical University of Lisbon, 1049-001 Lisboa, Portugal

We study a seesaw-type extension of the Standard Model in which the symmetry group is enlarged by a global $U(1)$. We introduce adequate scalar and fermion representations which naturally explain the smallness of neutrino masses. With the addition of a viable scalar Dark Matter candidate, an original scenario of leptogenesis emerges. We solve the relevant set of Boltzmann equations and show how leptogenesis can be successfully implemented at the TeV scale. The constraints on the scalar mass spectrum are derived and the Dark Matter phenomenology is discussed.

Contents

*Electronic address: fxjossemichaux@gmail.com
†Electronic address: emiliano.molinaro@ist.utl.pt

I. INTRODUCTION

Now that we entered in the LHC era, the Standard Model (SM) of elementary particles can be definitively tested. Until now, the SM has been extremely successful, as no strong signals of new physics have been observed so far at particle accelerators. However other experiments have long-time evidences for the need of extensions of the SM particle content. Neutrino oscillations are the prime among them on the particle side, but the compelling gravitational evidences for the existence of Dark Matter (DM), as well as the observation of a matter-antimatter asymmetry in the Universe all call for new physics.

From neutrino oscillation experiments we know that at least two neutrinos should be massive with an overall mass scale m_ν constrained by different observations: $m_\nu \lesssim 1$ eV. More precisely, experiments with solar, atmospheric, reactor and accelerator neutrinos [1]-[10] set two mass scales in the theory, $\Delta m^2_\odot$ and $\Delta m^2_{\rm A}$, which drive the solar and atmospheric neutrino oscillations, respectively [11]:

$$\Delta m^2_\odot \, = \left(7.59^{+0.20}_{-0.21}\right) \times 10^{-5}\ {\rm eV}^2 \ , \qquad \Delta m^2_{\rm A} \, = \, (2.43 \pm 0.13) \times 10^{-3}\ {\rm eV}^2 \, . \tag{1.1}$$

Moreover, these experiments show that flavor neutrino mixing, described in terms of the PMNS [12–14] matrix, is characterized by two large mixing angles, θ_{12} and θ_{23}, and a small one, θ_{13} [15].

On the cosmological side, the matter content of the Universe has been measured with precision by WMAP [16]. The resulting Dark Matter and baryon number densities, $\Omega_{\rm DM}$ and $\Omega_{\rm B}$, are

$$\Omega_{\rm DM} = 0.229 \pm 0.015 \, , \quad \Omega_{\rm B} = 0.0458 \pm 0.0016 \, . \tag{1.2}$$

Several gravitational observations confirm the existence of non-baryonic matter [17], which is not accounted for in the SM. New physics extensions are then necessary and various viable DM candidates exist [17]. However, the real nature of DM is still elusive, as no direct proof has been observed - or firmly confirmed - so far [18]-[21]. The measurement by WMAP of the baryonic matter content of the Universe is in agreement with the value predicted by Big-Bang Nucleosynthesis from the observations of the primordial abundances [22]. However, an excess of baryons over antibaryons is observed, and the standard cosmological scenario fails to explain this Baryon Asymmetry of the Universe (BAU). Particle physics extensions of the SM are advocated to justify this: in relation with neutrino masses, the leptogenesis scenario [23, 24] constitutes one of the most elegant solutions.

In this paper we study a minimal extension of the SM in which it is possible to address, in a consistent way, the three puzzles listed above. The model is based on a global $U(1)_{B-\tilde{L}}$ symmetry, which is spontaneously broken below the electroweak symmetry breaking (EWSB) scale. The $\tilde{L}$ charge is a generalization of the usual lepton number L, as $\tilde{L} = L$ for the SM particles. The light neutrino masses are explained within a seesaw framework [25], through the introduction of a SM singlet Dirac fermion N_D, together with three Brout-Englert-Higgs scalar particles: two $SU(2)_W$ doublets $H_{1,2}$ and a SM singlet H_3, which drive the EWSB by acquiring non-zero vacuum expectation values (vevs). All these extra degrees of freedom are charged under the global $U(1)_{B-\tilde{L}}$ symmetry. In *e.g.* [26], neutrino masses were generated in models with similar scalar spectrum and/or based on a (spontaneously broken) global symmetry, although in different physical frameworks. In our scenario, when the seesaw scale is set in the TeV-range, such a particle content provides a UV-completion of the inverse-seesaw mechanism of neutrino mass generation [27].

Nevertheless, with just this particle content, neither the observed amount of baryon asymmetry nor the Dark Matter abundance, eq. (1.2), can be accounted for.

In order to solve also these two important issues, we complete the model by introducing a Majorana neutrino N_3 and a complex scalar S. Both particles are SM singlets, although S is charged under the global $U(1)_{B-\tilde{L}}$. The particle content of the model is summarized in Tab. I, together with the $U(1)_{B-\tilde{L}}$ quantum numbers of the fields. The new scalar S provides, after the breaking of $U(1)_{B-\tilde{L}}$, a natural Dark Matter candidate, whose stability is guaranteed by a remnant $\mathcal{Z}_2$ symmetry.

It is remarkable that the introduction of S allows a TeV scale scenario of leptogenesis. Indeed, as the Majorana field N_3 couples to N_D and S, the out-of-equilibrium CP-violating decays of N_3 can generate a number density asymmetry in N_D and S, resembling the standard thermal leptogenesis mechanism in the type I seesaw extension of the SM. However, in the present case leptogenesis is implemented in two steps: first an asymmetry in N_D and S is generated by the decays of N_3; in a second phase, the Dirac neutrino asymmetry is transferred to SM leptons by sufficiently fast neutrino Yukawa interactions. The latter set a link between successful leptogenesis and viable neutrino mass generation via the seesaw mechanism. Finally, as in standard leptogenesis, non-perturbative sphaleron effects partly convert this lepton asymmetry into a net baryon number [28].

In Section II we discuss neutrino mass generation through the (inverse) seesaw mechanism. In the subsequent Section III we tackle the problem of the BAU and study the constraints on the parameter-space of the model imposed by successful leptogenesis. The computation of the CP asymmetry and the set of coupled Boltzmann equations governing the number density evolutions are reported in the final appendices. In Section IV we discuss the scalar

Field	ℓ_α	$e_{R\alpha}$	N_D	N_3	H_1	H_2	H_3	S
$B-\tilde{L}$	-1	-1	-1	0	0	2	-2	-1

TABLE I: Charge assignment of the fields.

sector of the theory, deriving the mass spectrum and corresponding constraints. In Section V we study the possibility of having a viable Dark Matter in the model and comment on the possible observation of DM in direct detection experiments. Finally, in the last section we summarize the main results of the paper.

II. NEUTRINO MASSES WITH A GLOBAL $U(1)_{B-\tilde{L}}$

An effective Majorana neutrino mass term is generated below the EWSB scale from the following part of the interaction Lagrangian:

$$-\mathcal{L}_{\rm int} \supset M\,\overline{N}_D N_D + \left(y_1^i\,\overline{N}_D\,\widetilde{H}_1^\dagger\,\ell_i + y_2^j\,\overline{N}_D^c\,\widetilde{H}_2^\dagger\,\ell_j + \frac{\alpha}{\sqrt{2}}\,H_3\,\overline{N}_D\,N_D^c + \text{h.c.}\right), \tag{2.1}$$

where $\ell_i = (\nu_{i\,L}, e_{iL})^T$ $(i = e,\mu,\tau)$, $N_D^c \equiv C\overline{N}_D^T$ and $\widetilde{H}_k \equiv -i\sigma_2 H_k^*$ $(k = 1,2)$. [1] The coupling constant α and the neutrino Yukawa couplings $y_{1,2}^i$ are complex parameters. As we will see in the following, the phase of α plays a crucial role in the generation of the CP asymmetry necessary for the production of the observed amount of BAU.

The terms reported in the Lagrangian (2.1) provide a dynamical realization of the inverse seesaw mechanism [27] for the generation of neutrino masses in the case the mass of the Dirac field N_D is taken in the TeV-range. More specifically, in our scenario the standard lepton charge L is explicitly violated by the interactions involving the couplings y_2^i and α. Consequently, we expect that the active neutrino masses, generated through the (inverse) seesaw mechanism, do directly depend on these parameters. The model, in this minimal form, predicts two massive and one massless active neutrinos.

The seesaw mass scale M is a free parameter of the theory and can assume arbitrarily large values above the EWSB scale. However, in the following we will be mostly interested in the case where M is taken at the TeV scale. At energies much smaller than M, N_D is integrated out and we get at second order in $1/M$ the $(B-\tilde{L})$-conserving effective Lagrangian: [2]

$$\begin{aligned} -\mathcal{L}_{\rm eff} \supset & -\frac{y_1^i y_2^j + y_1^j y_2^i}{2M}\left(\overline{\ell}_j^c\,\widetilde{H}_2^*\right)\left(\widetilde{H}_1^\dagger\,\ell_i\right) + \frac{y_1^i y_1^j \alpha^*}{\sqrt{2}M^2}\left(\overline{\ell}_j^c\,\widetilde{H}_1^*\right)\left(\widetilde{H}_1^\dagger\,\ell_i\right) H_3^* \\ & + \frac{y_2^i y_2^j \alpha}{\sqrt{2}M^2}\left(\overline{\ell}_j^c\,\widetilde{H}_2^*\right)\left(\widetilde{H}_2^\dagger\,\ell_i\right) H_3 + \text{h.c.}\,, \end{aligned} \tag{2.2}$$

where the sum over the flavor indices i and j is understood. When the neutral components of the scalar fields H_k $(k = 1,2,3)$ take a non-zero vev, the operators in (2.2) generate a Majorana mass term for the flavor neutrino fields $\nu_{i\,L}$. Indeed, taking $\langle H_i\rangle = \left(0,\, v_i/\sqrt{2}\right)^T$ $(i = 1,2)$ and $\langle H_3\rangle = v_3/\sqrt{2}$ in (2.2), we obtain the neutrino mass Lagrangian

$$\mathcal{L}_{m_\nu} = -\frac{1}{2}\overline{\nu_{\mathbf{R}}^{\mathbf{c}}}\,m_\nu\,\nu_{\mathbf{L}} + \text{h.c.}\,, \tag{2.3}$$

where $\nu_{\mathbf{L}} \equiv (\nu_{eL}, \nu_{\mu L}, \nu_{\tau L})$, $\nu_{\mathbf{R}}^{\mathbf{c}} \equiv C\overline{\nu}_{\mathbf{L}}{}^T$ and

$$(m_\nu)_{ij} = -\left(y_1^i\,y_2^j + y_2^i\,y_1^j - y_1^i\,y_1^j\,\alpha^*\,\frac{v_1\,v_3}{v_2\,M} - y_2^i\,y_2^j\,\alpha\,\frac{v_2\,v_3}{v_1\,M}\right)\frac{v_1\,v_2}{2\,M}\,. \tag{2.4}$$

---

[1] C is the usual charge conjugation matrix of Dirac spinors.

[2] We do not include flavor kinetic mixing terms in the Lagrangian (2.2), which arise by dimension 6 effective fermion operators.

The masses of the two active neutrinos are given by

$$m_\pm \;\simeq\; \frac{1}{4}\left| v_3 \frac{v_2^2}{M^2} y_2^2 \alpha + v_3 \frac{v_1^2}{M^2} y_1^2 \alpha^* - 2 v_1 \frac{v_2}{M} y_{12} \pm \sqrt{\left(v_3 \frac{v_2^2}{M^2} y_2^2 \alpha + v_3 \frac{v_1^2}{M^2} y_1^2 \alpha^* - 2 v_1 \frac{v_2}{M}\, y_{12} \right)^2 + 4\, v_1^2 \frac{v_2^2}{M^2} \eta_{12}^2} \right| , \quad (2.5)$$

where we define $y_{12} = y_1^e y_2^e + y_1^\mu y_2^\mu + y_1^\tau y_2^\tau$, $y_k = \sqrt{(y_k^e)^2 + (y_k^\mu)^2 + (y_k^\tau)^2}$ $(k = 1, 2)$ and $\eta_{12} = \sqrt{(y_1^e y_2^\mu - y_2^e y_1^\mu)^2 + (y_1^e y_2^\tau - y_2^e y_1^\tau)^2 + (y_1^\mu y_2^\tau - y_2^\mu y_1^\tau)^2}$. As usual in two-Higgs doublet models, the vevs of the two scalar doublets, v_1 and v_2, are related to the EWSB scale: $\sqrt{v_1^2 + v_2^2} \equiv v \simeq 246$ GeV. As explained in Section IV, the hierarchy among the Higgs vevs is tightly constrained in our model, in particular from the presence of a massless Goldstone boson associated with the spontaneous breaking of the global $U(1)_{B-\tilde{L}}$: phenomenological constraints enforce $v_2 \ll v_{1,3}$, and by convention we impose $v_3 \leq v$. As we will see in Section IV, this hierarchical pattern is easily realized in the model. Typically, for $|\alpha| \approx 0.01$, $M \approx 1$ TeV and a scalar spectrum with $v_2 \approx 10$ MeV, $v_3 \approx 100$ GeV, the neutrino Yukawa couplings are $|y_{1,2}| \approx 10^{-4}$.

The Yukawa interaction $\alpha\, H_3\, \overline{N}_D\, N_D^c$ generates after EWSB a small Majorana mass term for the two chiral components of the Dirac field N_D, which is then split into two quasi-degenerate Majorana fermions: they behave as a pseudo-Dirac pair [29]-[31], with a mass difference of the order $2\, v_3\, |\alpha|$. Such scenarios have been studied in detail in [32], where it was shown that a high-level of degeneracy prevents the Majorana nature of these states to be observed at colliders, LHC included. Indirect signals of TeV scale pseudo-Dirac neutrinos coupled to charged leptons can in principle be observed both in lepton flavor violating processes, *e.g.* charged lepton radiative decays $\ell_i \to \ell_j\, \gamma$ and $\mu - e$ conversion in nuclei, and in experiments searching for lepton number violation, such as neutrinoless double beta decay processes. For these processes, the contribution of the heavy neutrinos to the decay rate may be relevant/dominant in the case of $M \approx (100 - 1000)$ GeV, $|\alpha| v_3 / M \approx 10^{-3} - 10^{-2}$ and for sizable neutrino Yukawa couplings, $|y_{1,2}| \approx 10^{-2}$ [33].

Finally, we remark that the coupling α is not strictly required in order to obtain two massive neutrinos, whereas the introduction of y_2 is mandatory. Actually, one can show that y_1 and y_2 are also sufficient to fully reconstruct the low-energy neutrino data, up to a normalization factor [34]. From eq. (2.5) we get the following relation:

$$|\eta_{12}|\; v_1\, v_2\, \frac{1}{M} \;=\; 2\, \left(\Delta m^2_{\odot}\, \Delta m^2_{\rm A} \right)^{1/4} . \quad (2.6)$$

This equation clearly shows that for $y_2 = 0$ or for $(y_2^e, y_2^\mu, y_2^\tau)$ aligned with $(y_1^e, y_1^\mu, y_1^\tau)$, $|\eta_{12}| = 0$ and only one neutrino is massive, in contradiction with neutrino oscillation data. Barring accidental cancellations, eq. (2.6) implies

$$|y_1|\, |y_2| \;\sim\; 2 \times 10^{-8} \left(\frac{M}{1\ \text{TeV}} \right) \left(\frac{10\ \text{MeV}}{v_2} \right) . \quad (2.7)$$

III. TWO-STEP LEPTOGENESIS

Before discussing how the baryon asymmetry is generated in our scenario, let us briefly recall the standard picture of leptogenesis, based on the type I seesaw extension of the Standard Model. For a detailed discussion, see [35] and references therein. In the standard scenario, at least 2 massive right-handed (RH) neutrinos, which are $SU(2)_W \times U(1)_Y$ singlets, are introduced and couple to lepton doublets through Yukawa interactions. These singlets are Majorana fermions whose mass M_R is not related to the electroweak scale and can assume arbitrarily large values. The RH neutrinos evolve together with the SM particles in a hot but expanding Universe; when the temperature drops down below M_R, they start to decouple and decay out-of-equilibrium in both leptons and antileptons. If CP is violated in these processes, a non-zero asymmetry is produced, which is subsequently converted into a net baryon number by fast sphaleron interactions. The latter are non-perturbative effects, in thermal equilibrium above the EWSB scale up to temperatures $T \lesssim 10^{12}$-10^{13} GeV [36]. Several interactions should be considered for an accurate determination of the efficiency of leptogenesis in producing a baryon asymmetry. Spectator processes play an important role in modifying the production/depletion mechanisms, most notably by spreading the lepton asymmetry into different species.

In the present case, given the particle content and the charge assignment listed in Tab I, the interaction Lagrangian receives, besides the operators of the seesaw sector in eq. (2.1), contributions from the extra Majorana field N_3 and the scalar S:

$$-\,\mathcal{L}_{\rm int} \;\supset\; \mu_S^2\, S^* S \,+\, \frac{1}{2} M_3\, \overline{N}_3\, N_3^c \,+\, \left(g\, S\, \overline{N}_D\, N_3 \,-\, \frac{\mu''}{\sqrt{2}} S^2 H_3^* \,+\, \text{h.c.} \right) , \quad (3.1)$$

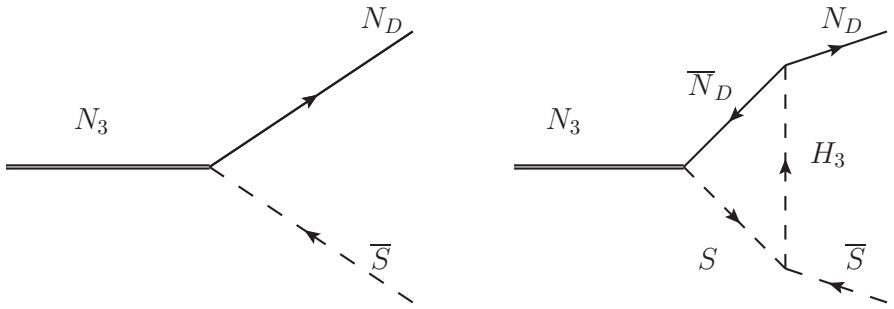

FIG. 1: Diagrams contributing to the CP asymmetry in the decays of N_3.

where M_3, μ'' and g can be set real by a redefinition of the phases of N_3, S and H_3. We impose N_3 to be heavier than N_D and S.

In this model, the generation of a baryon asymmetry proceeds in two different phases. In a first phase, which is similar to the standard leptogenesis scenario, an asymmetry in Dirac neutrinos N_D and in S is generated by the out-of-equilibrium decays of the Majorana field N_3. As we describe below, the CP asymmetry in N_3 decays is only possible after the introduction of S, carrying the same $B-\tilde{L}$ quantum number as N_D.

Besides decays and inverse decays, several scatterings affect N_D and S asymmetries. All these interactions conserve the total $B-\tilde{L}$ charge. In a second phase, owing to the neutrino Yukawa couplings, the produced N_D and S asymmetries are transferred and reprocessed into a lepton asymmetry. In this second phase, the sphaleron processes partly convert the so produced lepton asymmetry into a final baryon number, as in the standard picture.

This model can thus be viewed as the SM augmented with a second Higgs doublet, combined with a hidden sector composed of the fields N_3, S and H_3. The two sectors share a conserved $B-\tilde{L}$ charge through the Dirac neutrino N_D. In that extent, the role of the neutrino Yukawa couplings is central both in the generation of light neutrino masses and in the production of a BAU, in agreement with observations.

A. The CP asymmetry ϵ_{CP}

In the standard leptogenesis scenario a CP asymmetry is generated by the interference between the tree-level and the one-loop corrections to the decay amplitude of the heavy Majorana neutrinos [24, 37], owing to the presence of at least two heavy states. In our case, with only one heavy neutrino N_D, no CP violation is produced in N_D decays. On the other hand, a non-zero CP asymmetry can be generated by the addition of N_3 and S, from the interference between the tree-level and one-loop correction to N_3 decay amplitude, whose Feynman diagrams are depicted in Fig. 1.

The detailed computation of the CP asymmetry in N_3 decays is provided in Appendix B. We report below the resulting expression in the limit $M_3 \gg M, \mu_S$:

$$\epsilon_{CP} \simeq -\frac{\mathrm{Im}(\alpha)}{16\pi}\,\frac{\mu''}{M_3}\,. \tag{3.2}$$

Despite of the fact that N_3 decays depend on the coupling constant g, the latter being a real parameter does not enter in the expression of ϵ_{CP}, cf. eq. (B13). The only source of CP violation relevant for leptogenesis is the phase of the complex parameter α in the Lagrangian (3.1). It is remarkable that, in contrast to the standard leptogenesis scenario, there is no direct dependence of ϵ_{CP} on the neutrino Yukawa couplings $y_{1,2}$. Still, a connection between the leptogenesis CP-violating phase and the light neutrino masses exists and is actually provided by the imaginary part of α. We remark that the parameter μ'' in (3.2) enters in the mass splitting between the real and imaginary parts of S (cf. eq. (5.1)) and therefore determines which is the DM candidate of the model, as shown in Section V. Provided μ'' is not too much suppressed compared to M_3 and the phase of α is different from zero, ϵ_{CP} takes sizable values. We typically have:

$$\epsilon_{CP} \simeq -2\times 10^{-6}\left(\frac{\mu''}{1\,\mathrm{GeV}}\right)\left(\frac{10\ \mathrm{TeV}}{M_3}\right)\mathrm{Im}(\alpha)\,. \tag{3.3}$$

B. Asymmetry productions

We discuss now the salient aspects of leptogenesis in our scenario. We eventually distinguish between two stages of production, but we shall emphasize that these stages are not necessarily consecutive and may occur in the same temperature range.

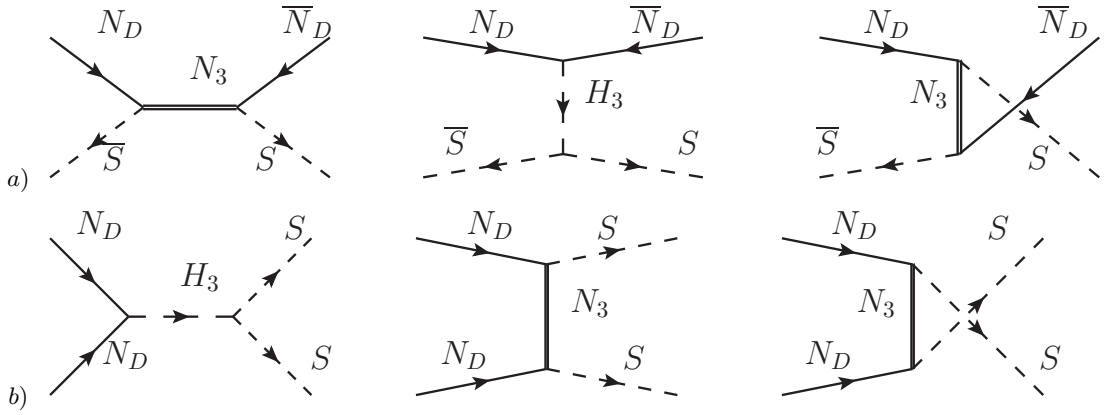

FIG. 2: Feynman diagrams of the $\Delta N_D = \Delta S = 2$ scatterings.

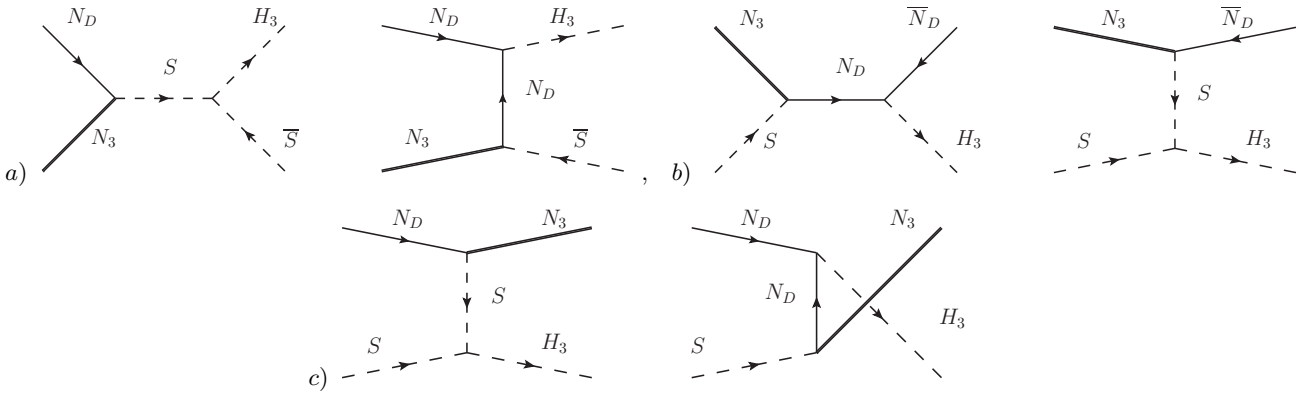

FIG. 3: Feynman diagrams of the $\Delta N_D = \Delta S = 1$ scatterings.

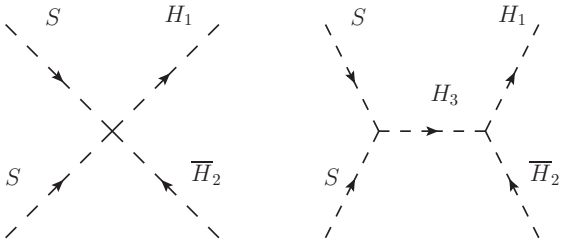

FIG. 4: Feynman diagram of the S self-annihilation.

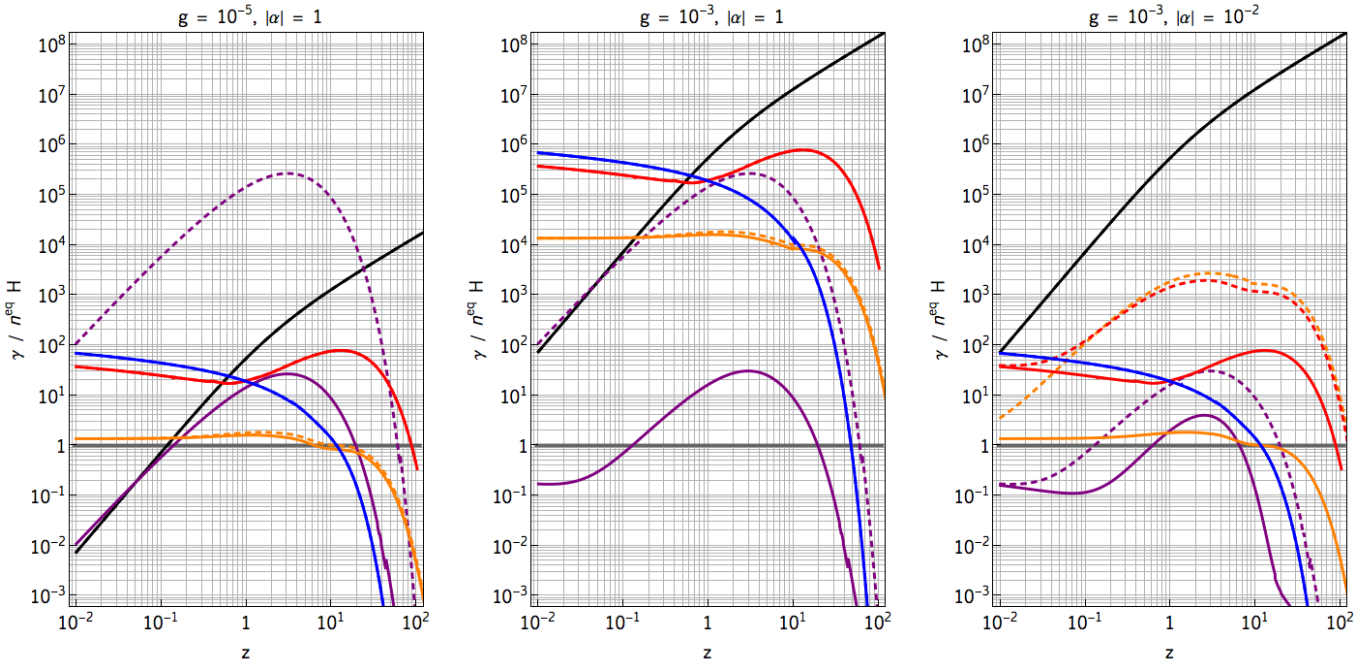

FIG. 5: Processes relevant in the first stage of leptogenesis: thermal density rates as function of $z \equiv M_3/T$, for $M_3 = 50$ TeV, $M = 10$ TeV and $\mu'' = 1(100)$ GeV, plain (dashed) curves. In black is reported the total decay rate of N_3. The purple curves stand for the sum of the (non-resonant part of the) diagram a) and diagram b) in Fig. 2. The blue, orange and red curves correspond, respectively, to the processes a), b) and c) shown in Fig. 3.

1. *First Stage: processes at $\mathcal{O}(\alpha^2)$, $\mathcal{O}(g^2)$, $\mathcal{O}(g^2\,\alpha^2)$ and $\mathcal{O}(g^4)$.*

We list below the processes relevant in the first step, where the asymmetries in S and N_D are created. [3] Further details are given in Appendix C:

- Decays and inverse decays of N_3: $N_3 \to N_D\,\overline{S}\,, \overline{N}_D\,S$ (see Fig. 1).
- $\Delta N_D = \Delta S = 2$ scatterings: $N_D\,\overline{S} \leftrightarrow \overline{N}_D\,S$ and $N_D\,N_D \leftrightarrow S\,S$ (see Fig. 2).
- $\Delta N_D = \Delta S = 1$ scatterings: $N_D\,N_3 \leftrightarrow H_3\,\overline{S}$, $N_D\,\overline{H}_3 \leftrightarrow N_3\,\overline{S}$ and $N_D\,S \leftrightarrow N_3\,H_3$ (see Fig. 3).
- S self-annihilation: $S\,S \leftrightarrow H_1\,\overline{H}_2$ (see Fig. 4).

Notice that the last process depends on interaction terms reported in the scalar potential of the model (see eq. (4.3)). However, it turns out to be numerically irrelevant, so we disregard the effect of this term in the following.

We display in Fig. 5 the interaction rates γ^{eq} of some of the up-listed processes as function of the parameter $z \equiv M_3/T$, where T is the temperature of the plasma. These rates are normalized by $H(z)\,n^{eq}_{N_3}(z)$, except for the $\Delta N_D = 2$ rates which are normalized by $H(z)\,n^{eq}_{N_D}(z)$, as they only act as damping terms. [4] For illustration we fix $M_3 = 50\,\text{TeV}$, $M = 10\,\text{TeV}$ and we choose representative values of g and $|\alpha|$ for the different panels. [5]

We represent in each plot by straight (dashed) lines the computed rates assuming $\mu'' = 1\,(100)\,\text{GeV}$. For $\mu'' = 1\,\text{GeV}$, the cross-sections of the $\Delta N_D = 2$ scatterings a) are dominated by their s- and u-channels and scale as $\mathcal{O}(g^4)$. The

[3] We denote by ΔX the absolute variation of the X particle number density.
[4] In Fig. 5 only the off-shell part of the $\Delta N_D = 2$ diagrams a) is shown, as its on-shell part equals $\gamma_D/4$, γ_D being the total decay rate of N_3.
[5] For definiteness, in the following numerical evaluations we set the phase of α to its maximum value $\alpha = -\mathrm{i}\,|\alpha|$.

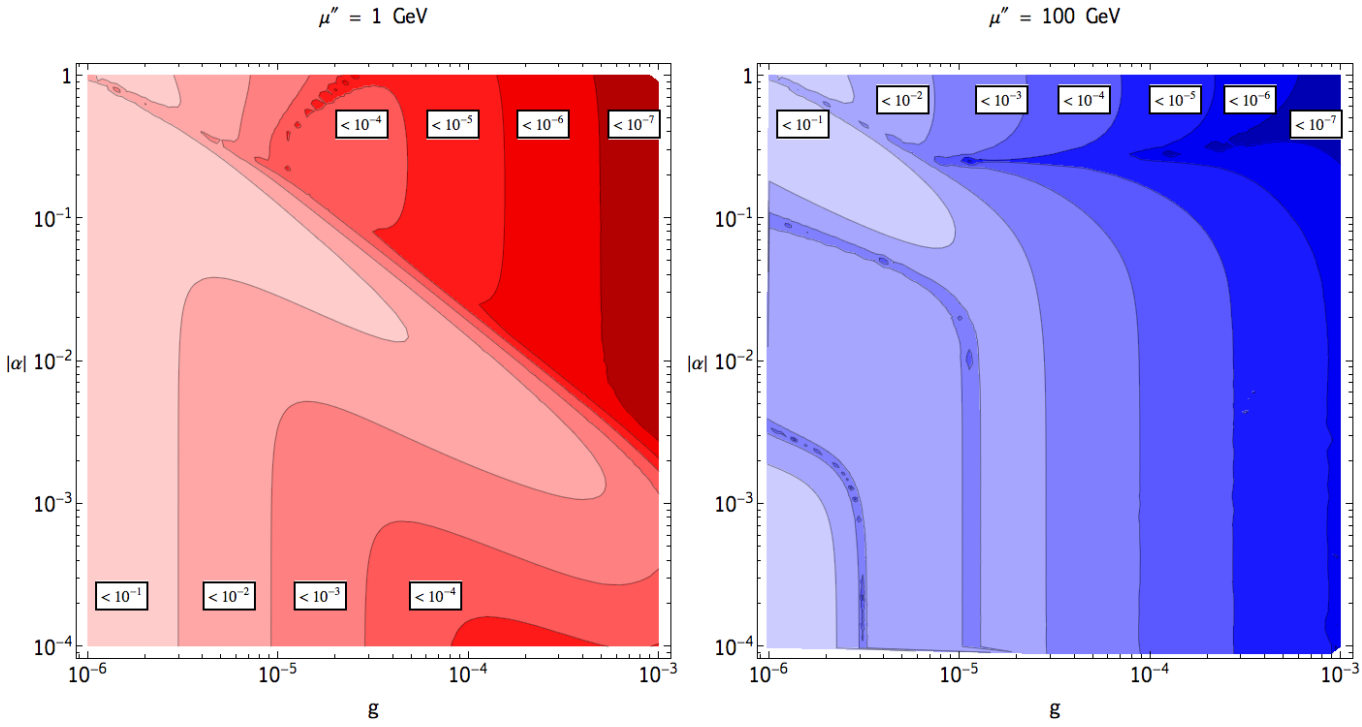

FIG. 6: Efficiency η_1 of production of N_D asymmetry in the first stage of leptogenesis, cf. eq. (3.4), as a function of g and $|\alpha|$ for $M_3 = 50\,\text{TeV}$, $M = 10\,\text{TeV}$ and $\mu'' = 1(100)\,\text{GeV}$ in the left (right) panel.

$\Delta N_D = 2$ scatterings b) on the other hand are governed by their s-channel and are proportional to $|\alpha|^2\,\mu''^2$. The $\Delta N_D = 1$ processes a), b) and c) of Fig. 3 are dominated by their respective t-, s- and u-channels and therefore scale as $\mathcal{O}(g^2\,|\alpha|^2)$. For larger values of μ'', *e.g.* $\mu'' = 100\,\text{GeV}$, the $\Delta N_D = 1$ processes b) and c) get sizable contributions from their t-channels ($\propto g^2\,\mu''^2$) which dominate over the other channels for small values of α, as can be seen in the right panel of Fig. 5. The different interaction rates where evaluated using the packages FeynArts [38] and FormCalc [39]. To this end, we implemented our model, $\mathcal{L}_{\text{int}}$ eq. (A1), via FeynRules [40].

The various interactions considered above control the amount of N_D and S asymmetries produced during the first stage of leptogenesis. As the lepton asymmetry -and finally the baryon asymmetry- mostly depends on the amount of N_D asymmetry produced in the first step, it is useful to introduce an efficiency factor η_1 defined through:

$$Y_{\Delta N_D}(z_{tr}) = \epsilon_{CP}\,\eta_1\,Y^{eq}_{N_3}(T \gg M_3)\,. \tag{3.4}$$

In this parametrization, Y_X indicates the comoving number density of X, while $z_{tr} \sim M_3/M$ approximately marks the transition between the first and second stage: for $z \gtrsim z_{tr}$, *i.e.* $T \lesssim M$, N_D decouples from the plasma and decays into leptons and antileptons.

Given the numerous interactions considered above, the derivation of an analytic expression for the efficiency factor η_1 is quite challenging. Nevertheless, we perform a numerical evaluation of η_1 by solving the set of Boltzmann equations reported in Appendix C. The resulting efficiency is shown in Fig. 6, where iso-contours of η_1 in the $g - |\alpha|$ plane are displayed, for $M_3 = 50\,\text{TeV}$, $M = 10\,\text{TeV}$ and $\mu'' = 1\,\text{GeV}$ (100 GeV) in the left (right) panel.

We first consider the case of small μ'', left panel of Fig. 6. In this case, the $\Delta N_D = 2$ scatterings are typically smaller than the decays and inverse decays, as shown in Fig. 5. Depending on the value of α, the $\Delta N_D = 1$ scattering rates $\gamma^k_{N_3}$ ($k = a, b, c$), may be in equilibrium when the N_D asymmetry is produced. This occurs if

$$\frac{\gamma^k_{N_3}}{n^{eq}_{N_D}\,H(M_3)} \gtrsim 1 \quad \Longrightarrow \quad |\alpha| \times \left(\frac{g}{10^{-6}}\right) \gtrsim 1\,. \tag{3.5}$$

As can be seen in the left panel of Fig. 6, the efficiency η_1 strongly depends on whether the ΔN_D scatterings are in equilibrium at $T \sim M_3$ or not. In the case their rates are not fast enough, *i.e.* if the condition (3.5) is not satisfied, the production of N_D and S asymmetries is mostly driven by decays and inverse decays of N_3. This situation is very similar to the standard leptogenesis scenario, when $\Delta L = 1$ scatterings are neglected. Therefore, we expect that larger

values of the coupling g increase the washout effects. The strength of N_3 decays and inverse decays can be expressed in terms of the washout parameter K_D

$$K_D \equiv \frac{\Gamma_{N_3}}{H(M_3)} \simeq 2 \left(\frac{g}{10^{-6}}\right)^2 \left(\frac{50\,\mathrm{TeV}}{M_3}\right) . \tag{3.6}$$

For $g \gtrsim 10^{-6}$ and $M_3 \sim \mathcal{O}(10)\,\mathrm{TeV}$, decays and inverse decays act in a strong washout regime, where the efficiency is approximately given by [41]:

$$\eta_1 \sim \frac{0.4}{K_D\,\log(K_D)} . \tag{3.7}$$

For smaller values of g, decays and inverse decays act in a weak washout regime, and the efficiency scales as K_D^2 [41], in the case where the abundance of N_3 is vanishing at high temperatures.

In the opposite regime, when the $\Delta N_D = 1$ scatterings are fast enough and the condition eq. (3.5) is satisfied, an initial (anti-)asymmetry is produced at earlier times, due to the CP violation in scatterings, which is discussed in Appendix C. From Fig. 6, we can distinguish two relevant cases, according to the values of α and g. For $|\alpha| \approx 10^{-6}/g$, the $\Delta N_D = 1$ scatterings essentially act as source terms, producing N_D and S asymmetries, thereby increasing the efficiency η_1. This effect is manifest in the diagonal of the left plot of Fig. 6. Conversely, for larger values of α, the $\Delta N_D = 1$ scatterings act as damping terms and increase the washout of the asymmetries. The resulting efficiency is therefore highly reduced.

The case of a larger μ'' is depicted in the right panel of Fig. 6, where we fix $\mu'' = 100\,\mathrm{GeV}$, while M_3 and M assume the same values as before. As already stated, in this case the $\Delta N_D = 1$ scatterings b) and c) pick-up sizable contributions from their corresponding t-channels, and are enhanced for relatively small values of α, compared to the $\mu'' = 1$ GeV case, as can be seen in the right panel of Fig. 5. For $|\alpha| \lesssim 0.1$, the efficiency depends essentially on g, since the scatterings are negligible with respect to the decays and inverse decays, and then η_1 behaves as in eq. (3.7). However, for small values of g, $g \lesssim \text{few}\,10^{-5}$, $\Delta N_D = 1$ scatterings become competitive with decays and inverse decays, both in the generation and in the washout of N_D and S asymmetries. For values of α of order one and small g, the scatterings mainly act as source terms in analogy with the $\mu'' = 1$ GeV regime, thus increasing η_1.

We see that in this first stage, the efficiency of N_D and S asymmetry production can be close to its maximum possible value in a large region of the parameter-space. However, this does not guarantee a successful leptogenesis, as this asymmetry should be transferred efficiently to leptons.

2. *Second Stage: processes at $\mathcal{O}(y_{1,2}^2)$, $\mathcal{O}(g^2\,y_{1,2}^2)$.*

We now concentrate on the second step of leptogenesis: the transfer of N_D asymmetry to the lepton doublets. Once a lepton asymmetry is generated, the sphaleron processes which are active at the leptogenesis epoch convert part of it into a non-zero baryon number density. The second stage ends at the freeze-out of the sphalerons, that may occur before or right after EWSB [42].

We report below the main $\Delta\ell = 1$ processes which participate in the lepton charge transfer mechanism:

- Decays of N_D, which are either L-conserving, $N_D \to \ell\,H_1$, or L-violating, $N_D \to \overline{\ell}\,\overline{H}_2$.
- Scatterings on top quarks: the s-channel $N_D\,\overline{\ell} \leftrightarrow \overline{t}\,q_3$ and the t-channels $N_D\,q_3\,(\overline{t}) \leftrightarrow \ell\,t\,(\overline{q_3})$. These processes are mediated by the exchange of the Higgs doublet H_1 and correspond to the $\Delta L = 1$ scatterings in standard leptogenesis. Notice, however, that in our case lepton number is conserved.
- Scatterings on N_3: $N_3\,S \leftrightarrow \ell\,H_1$ and $N_3\,S \leftrightarrow \overline{\ell}\,\overline{H}_2$ which are mediated by N_D. A CP asymmetry emerges from these processes, as shown in Appendix C.

We do not include the scatterings involving gauge bosons in our evaluation of the baryon asymmetry. However, we do not expect these processes to have a quantitative impact. Indeed, they cannot act as a source term for the lepton asymmetry since no CP violation is possible in this case, in contrast to the standard leptogenesis scenario [43]. In addition, they tend to equilibrate the lepton and N_D number densities, like the scatterings on top quarks considered above. Actually, it is shown in references [44]-[45] that these processes have comparable rates.

The lepton doublet can also participate in $\Delta L = 2$ N_D-mediated scatterings, similarly to the standard leptogenesis case: $\ell\,H_1 \leftrightarrow \overline{\ell}\,\overline{H}_2$ and $\ell\,\ell \leftrightarrow \overline{H}_1\,\overline{H}_2$. In this case the scattering rate is proportional to both the neutrino Yukawa couplings, y_1 and y_2. In a democratic scenario, that is for $|y_1| \approx |y_2|$, provided the constraints from active neutrino masses, eqs (2.5) and (2.6) are satisfied, such $\Delta L = 2$ scatterings are usually in equilibrium at the leptogenesis time.

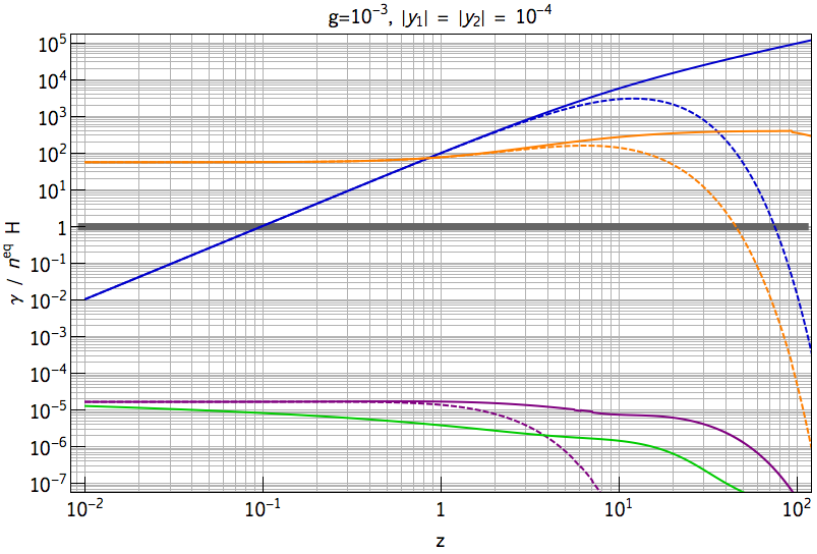

FIG. 7: Processes relevant in the second stage of leptogenesis: thermal density rates γ^{eq} as function of $z \equiv M_3/T$, for $M_3 = 50\,\text{TeV}$, $M = 10\,\text{TeV}$. The blue curves stand for decays of N_D. The orange curves stand for the (sum of s- and t-channel) $\Delta\ell = 1$ scatterings on top quarks, while the purple ones represent $\Delta\ell = 1$ scatterings on N_3. The green line corresponds to the total $\Delta L = 2$ scattering rate.

They are however greatly suppressed compared to the $\Delta\ell = 1$ scatterings and turn out to be numerically irrelevant, as illustrated below.

In this second stage, all interactions depend on the neutrino Yukawa couplings y_1 and y_2. In the limit where these couplings are zero, no lepton (doublet) asymmetry can be generated as basically both N_D and S decouple from the SM sector. This clearly implies a lower bound on the values of y_1 and y_2.

Let us discuss this bound, independently of the constraints from low-energy neutrino masses, as it sheds light on how this second stage works. To this end, we represent in Fig. 7 the processes relevant in the second step for the same set of parameters used in Fig. 5: $M_3 = 50\,\text{TeV}$, $M = 10\,\text{TeV}$ and $g = 10^{-3}$, and for $|y_1| = |y_2| = 10^{-4}$. We represent in Fig. 7 by plain (dashed) curves the rates normalized by $n_X^{eq}\,H(M)$, where $X = N_D$ (ℓ), acting as source (damping) terms. The blue curves correspond to N_D decays, both L-conserving and violating as $|y_1| = |y_2|$. The orange (purple) curves are related to scatterings on top (N_3), while the green line stands for the $\Delta L = 2$ processes. Scatterings on N_3 and $\Delta L = 2$ interactions are clearly sub-dominant and can be neglected.

A lower bound on y_1 can be derived by demanding that the scattering rates on top quarks, denoted by $\gamma^t_{N_D}$, are in equilibrium at $T \sim M$, when acting as a source term for the lepton asymmetry:

$$\frac{\gamma^t_{N_D}}{n^{eq}_{N_D}\,H(M)} \gtrsim 1 \quad \Longrightarrow \quad |y_1| \gtrsim 10^{-5} \times \sqrt{\frac{M}{10\ \text{TeV}}}\,. \tag{3.8}$$

Therefore, provided y_1 is large enough, the L-conserving scatterings are in equilibrium and can transfer the N_D asymmetry to the lepton doublets. A similar lower bound arises for y_2 from the corresponding $\Delta L = 1$ scatterings with gauge bosons.

The main source of lepton asymmetry production may originate just from the decays of N_D. Let us suppose, indeed, that the lower bound on y_1, eq. (3.8), is not satisfied. Still, as we see from Fig. 7, decays dominate over the scatterings at $T \sim M$. For these decays to be effective in redistributing the N_D asymmetry to leptons, the Dirac neutrino should be heavy enough, say $M \gtrsim 10 \times T_{sph}$, and the following condition should be satisfied:

$$\Gamma_{N_D} \gtrsim H(M) \quad \Longrightarrow \quad |y_{1,2}| \gtrsim 6 \times 10^{-7} \sqrt{\frac{M}{10\,\text{TeV}}}\,. \tag{3.9}$$

In summary, for neutrino Yukawa couplings smaller than the bound above, the lepton number asymmetry production is not efficient. if only condition (3.9) is satisfied, almost all N_D decays to leptons, and we expect that at the end of the second stage, the lepton asymmetry equals the amount of N_D asymmetry produced in the first stage. For larger Yukawa couplings satisfying eq. (3.8), $Y_{\Delta\ell}(z_{tr}) \approx Y_{\Delta N_D}(z_{tr})$ at the end of the first stage, so at the end of the second stage, $Y_{\Delta\ell}(z_{sph}) \approx 2\,Y_{\Delta N_D}(z_{tr})$.

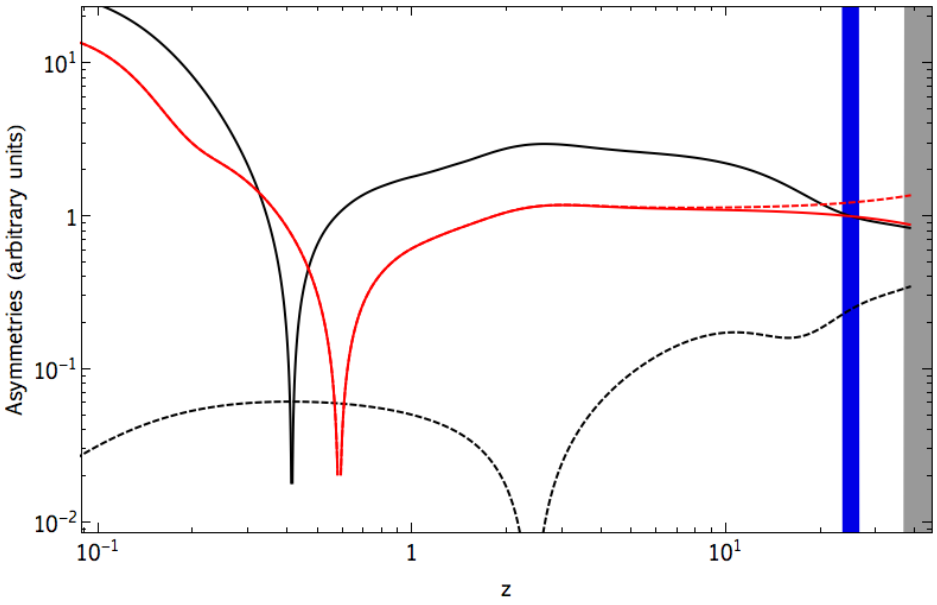

FIG. 8: Influence of scatterings on the transfer of N_D asymmetry to a lepton doublet asymmetry. See the text for details.

The case of a light Dirac Neutrino

An interesting case is realized when the Dirac neutrinos are so light that they don't have enough time to decay before the freeze-out of the sphalerons. Demanding that the scatterings with quarks are in equilibrium, at least slightly before the sphalerons decouple, the condition (3.8) is changed to $|y_1| \gtrsim 10^{-6}$. Therefore y_1 should be at least larger than the electron Yukawa coupling. We illustrate this remarkable case in Fig. 8, where we fix $M = 200\,\text{GeV}$ and we consider two sets of values for $|y_1|$ and $|y_2|$: *i)* $|y_1| = |y_2| = 5 \times 10^{-4}$ (red curves) and *ii)* $|y_1| = |y_2| = 5 \times 10^{-7}$ (black curves). Notice that the latter case may hardly be compatible with constraints from neutrino masses, eqs (2.5)-(2.7). The dashed and plain curves correspond to the lepton doublet and N_D asymmetries, respectively, and all the asymmetries have been normalized to $Y_{N_D}(z_{tr})$, where $z_{tr} \sim M_3/M$ is indicated by a blue band. We impose a sphaleron freeze-out at around $T_{sph} \sim 130\,\text{GeV}$, which is represented by the gray band.
We see from Fig. 8 that while N_D asymmetry is almost unaffected by the Yukawa hierarchy, in case *ii)* leptons do not equilibrate with N_D as scatterings are out-of-equilibrium, while in case *i)* $Y_{\Delta\ell} \approx Y_{\Delta N_D}$ at temperatures well above M.

Provided that the neutrino Yukawa couplings are sufficiently large, an asymmetry in N_D will be always transmitted to the lepton sector, regardless of the Dirac neutrino mass: we can therefore asset that no lower bound can be derived on M from leptogenesis.

In conclusion, once light neutrino mass constraints are applied, a lepton asymmetry is efficiently produced. A successful leptogenesis then only relies upon the amount of N_D asymmetry produced in the first stage.

C. Successful leptogenesis

In the former subsections, we analyzed the conditions under which a N_D asymmetry is efficiently produced during the first step of leptogenesis, and subsequently transmitted to the lepton doublets. Through the sphaleron processes, this lepton asymmetry is partly converted into a baryon number density. The sphalerons violate both lepton and baryon numbers, but conserve $B - L$: it is therefore more convenient to evaluate the $B - L$ asymmetry. Given the different processes in thermal equilibrium during leptogenesis era, the final baryon asymmetry reads:

$$Y_{\Delta B} = \frac{2}{7}\, Y_{\Delta(B-L)}(z_{sph})\,. \tag{3.10}$$

The derivation of eq. (3.10) is given in Appendix D. We illustrate in Fig. 9 the evolution of N_D, S and baryon

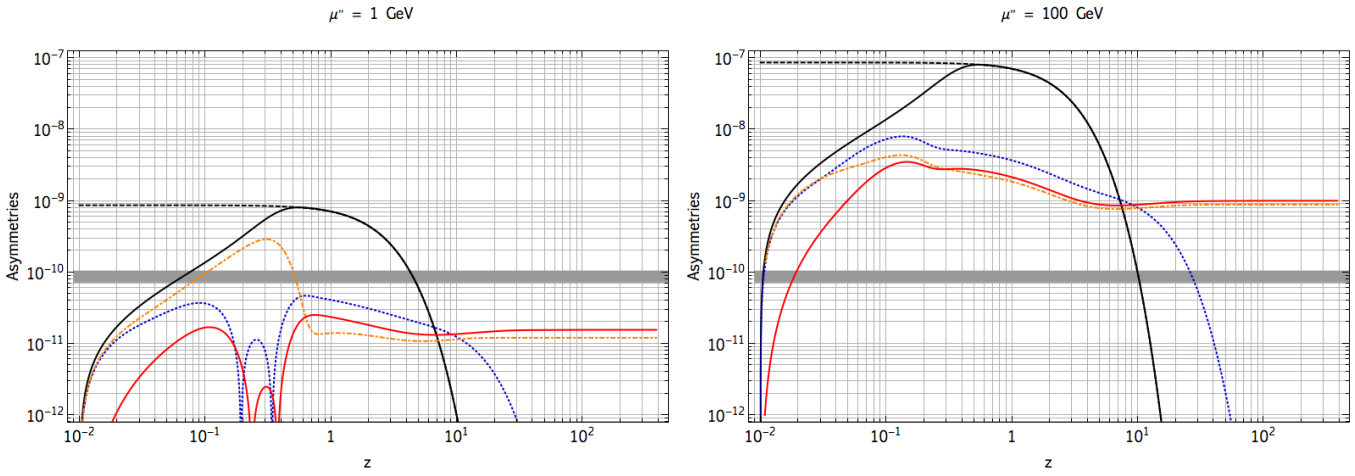

FIG. 9: Evolution of number density asymmetries in function of z. $M_3 = 50$ TeV, $M = 10$ TeV, $|\alpha| = 0.1$ and $g = 10^{-5}$ are fixed. The black plain (dashed) curves represent $\epsilon_{CP} \times Y_{N_3}^{(eq)}$. In dotted-blue, dot-dashed orange and plain red are shown $Y_{\Delta N_D}$, $Y_{\Delta S}$ and $Y_{\Delta B}$ respectively.

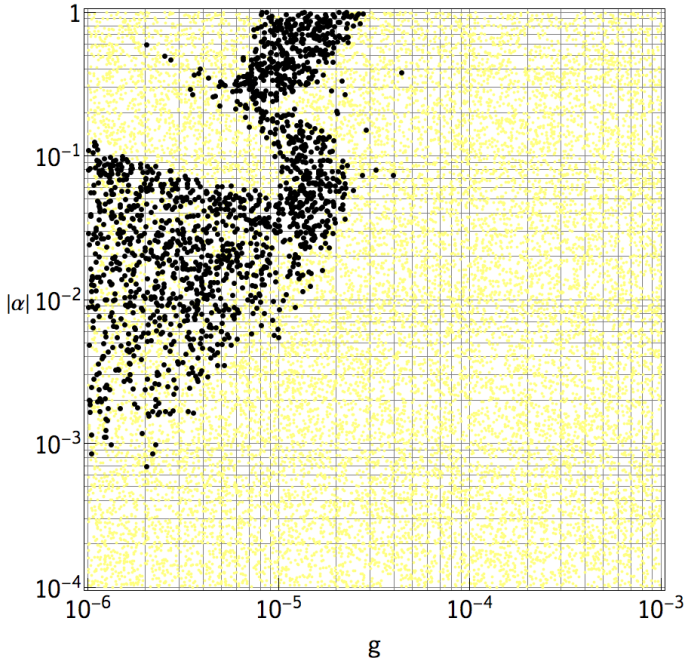

FIG. 10: Successful leptogenesis. Region of the parameter-space in the $|\alpha|$-g plane providing a final baryon asymmetry (not) compatible observations, (yellow) black points. We fix $M_3 = 50$ TeV, $M = 10$ TeV, $\mu_S = 100$ GeV and $\mu'' = 100$ GeV.

asymmetries against z for typical values of the parameters: $M_3 = 50$ TeV, $M = 10$ TeV, $\mu_S = 100$ GeV and $\mu'' = 1$ or 100 GeV, left or right panel respectively, for fixed values $|\alpha| = 0.1$ and $g = 10^{-5}$. For such values of $|\alpha|$ and g, we see from Fig. 6 that the efficiencies η_1 are quite similar, that is $\eta_1 \sim 0.1$. However, for $\mu'' = 100$ GeV the CP asymmetry is $\epsilon_{CP} \simeq 4 \times 10^{-6}$, two orders of magnitude larger than for $\mu'' = 1$ GeV, cf. eq. (3.2), and so the baryon asymmetry in the former case will be bigger. Indeed, for $\mu'' = 1$ GeV, $Y_{\Delta B} \approx 1.6 \times 10^{-11}$ while for $\mu'' = 100\,\text{GeV}$, $Y_{\Delta B} \approx 10^{-9}$. These values should be compared with the measurement of WMAP [16]:

$$Y_{\Delta B}^{\text{obs}} = (8.77 \pm 0.21) \times 10^{-11}\,. \tag{3.11}$$

In Fig. 10, we made a scan over the two parameters α and g: the black points represent values of $Y_{\Delta B}$ compatible with observations. [6] As we see, a successful leptogenesis is easily realized in our scenario, provided the CP asymmetry is big enough, that is $\epsilon_{CP} \gtrsim 3 \times 10^{-7}$, and the washout processes do not suppress the N_D asymmetry in the first stage, *i.e.* $\eta_1 \gtrsim$ few 10^{-3}.

IV. THE SCALAR SECTOR

Given the charge assignment of the scalar fields in Tab. I, the most general scalar potential $\mathcal{V}_{\rm SC}$ invariant under $SU(2)_W \times U(1)_Y \times \left[U(1)_{B-\tilde{L}}\right]$ can be written in the following form

$$\mathcal{V}_{\rm SC} \;\equiv\; \mathcal{V}_{\rm SB} \,+\, \mathcal{V}_{\rm DM}\,, \tag{4.1}$$

where $\mathcal{V}_{\rm SB}$ and $\mathcal{V}_{\rm DM}$ denote the symmetry breaking and dark matter scalar potentials, respectively:

$$\begin{aligned}
\mathcal{V}_{\rm SB} \;&=\; -\mu_1^2\, H_1^\dagger\, H_1 + \lambda_1\,(H_1^\dagger\, H_1)^2 - \mu_2^2\, H_2^\dagger\, H_2 + \lambda_2\,(H_2^\dagger\, H_2)^2 - \mu_3^2\, H_3^* H_3 + \lambda_3\,(H_3^* H_3)^2 \\
&+\; \kappa_{12}\, H_1^\dagger\, H_1 H_2^\dagger\, H_2 + \kappa'_{12}\, H_1^\dagger\, H_2 H_2^\dagger\, H_1 + \kappa_{13}\, H_1^\dagger\, H_1 H_3^* H_3 + \kappa_{23}\, H_2^\dagger\, H_2 H_3^* H_3 \\
&-\; \frac{\mu'}{\sqrt{2}}\left(H_1^\dagger\, H_2 H_3 + H_2^\dagger\, H_1 H_3^*\right)\,, \qquad (4.2) \\
\mathcal{V}_{\rm DM} \;&=\; \mu_S^2\, S^* S + \lambda_S\,(S^* S)^2 + \mathcal{F}_1\, H_1^\dagger\, H_1 S^* S + \mathcal{F}_2\, H_2^\dagger\, H_2 S^* S + \mathcal{F}_3\, H_3^* H_3 S^* S \\
&+\; h\, S^2 H_1^\dagger\, H_2 + h^*\, S^{*2} H_2^\dagger\, H_1 - \frac{\mu''}{\sqrt{2}}(S^2 H_3^* + S^{*2} H_3)\,. \qquad (4.3)
\end{aligned}$$

Through rotations of the scalar fields, all parameters but h can be made real, while the dimensional parameters are assumed positive. The parameter h is in general complex, but we will assume in the following that h is real.

The two scalar doublets $H_{1,2}$ and the complex scalar singlet H_3 are responsible for the breaking of $SU(2)_W \times U(1)_Y \times \left[U(1)_{B-\tilde{L}}\right]$ down to $U(1)_{em} \times [\mathcal{Z}_2]$. Given the charges of H_2 and H_3, the discrete $\mathcal{Z}_2$ emerges as a remnant symmetry of the global $U(1)_{B-\tilde{L}}$ after EWSB. Among the ten real scalar degrees of freedom, three of them are eaten through the Higgs mechanism, leaving a spectrum of seven physical scalars: two charged particles, $H^\pm$, two CP odd neutral scalars, A^0 and the massless Majoron $\mathcal{J}$ [46], and three CP even neutral scalars, h^0, H^0 and h_A. We derive in the following subsections some constraints on the scalar sector parameter-space. An exhaustive phenomenological study, although of great interest, is beyond the scope of this work.

The minimization of the scalar potential with respect to H_1, H_2 and H_3 vevs enforces three tree-level relations, that we use to define the quadratic terms μ_i. Indeed, by parametrizing the Brout-Englert-Higgs fields and S as

$$\begin{aligned}
H_k \;&=\; \left(H_k^+,\, \frac{v_k + h_k + \mathrm{i}\, a_k}{\sqrt{2}}\right)^T\,, \quad k = 1, 2\,, \qquad (4.4) \\
H_3 \;&=\; \frac{v_3 + h_3 + \mathrm{i}\, a_3}{\sqrt{2}}\,, \quad S = \frac{S_0 + \mathrm{i}\, S_1}{\sqrt{2}}\,, \qquad (4.5)
\end{aligned}$$

with

$$\langle H_i \rangle = \frac{v_i}{\sqrt{2}} \quad \text{and} \quad \langle S \rangle = 0\,, \tag{4.6}$$

we get the extremum conditions

$$\frac{\partial \mathcal{V}_{\rm SB}}{\partial v_i} = 0 \leftrightarrow \mu_i^2 = \frac{1}{2}\left(v_j^2 \tilde{\kappa}_{ij} + v_k^2 \kappa_{ik}\right) + 2\, v_i^2 \lambda_i - \frac{v_j v_k \mu'}{2 v_i}\,, \quad i, j, k = 1, 2, 3\,, \tag{4.7}$$

where $\tilde{\kappa}_{12} = \kappa_{12} + \kappa'_{12}$ and $\tilde{\kappa}_{ij} = \kappa_{ij}$ elsewhere. The extremum obtained in (4.7) is an absolute minimum provided the Hessian of $\mathcal{V}_{\rm SB}$ is positive definite. Boundedness from below of the scalar potential requires the quartic couplings λ_k to be positive, as well as a non-trivial relation among the couplings. Notice that, since both H_1 and H_2 are charged under $SU(2)_W \times U(1)_Y$, they both contribute to the masses of the SM gauge bosons.

---

[6] Actually, for the sake of illustration, we enlarge the required range, demanding $3 \times 10^{-11} \lesssim Y_{\Delta B} \lesssim 3 \times 10^{-10}$.

Among the numerous parameters of $\mathcal{V}_{\rm SC}$, it is worth to emphasize the role of the trilinear coupling μ'. In [47, 48], a two-Higgs doublet model was built invariant under a $U(1)$ global symmetry, explicitly broken by a term $\propto \mu^2 \phi_1^\dagger \phi_2$. Such term, for $\mu \ll v$ induces a type-II seesaw among the scalar vevs of ϕ_1 and ϕ_2: $\langle \phi_i \rangle \ll \langle \phi_j \rangle$, $i \neq j$. As noted in [48], such explicit breaking can be circumvented by the introduction of an additional scalar, say ϕ_3, whose vev generates the required term: $\mu^2 = \mu' \langle \phi_3 \rangle$. It is exactly along those lines that we build our scalar potential. Indeed, provided that μ' in (4.2) is suppressed, $\mu' \ll 1$ GeV, the minimization of $\mathcal{V}_{\rm SC}$ admits two possible hierarchical patterns for the vevs: $v_3 \ll v_{2,1}$ and $v_2 \ll v_{3,1}$. As we will show below, only the latter is physically viable. One may wonder about the naturalness of such a suppressed mass parameter μ'. Let us stress that very small values of μ' are actually technically natural. Indeed, this term, as well as the couplings h and y_2, are all terms linear in H_2. By setting them to zero, one actually enlarges the symmetry group by an extra $U(1)$ factor. Therefore, small values of these parameters are natural, in the 't Hooft sense [49].

A. *CP* odd neutral scalars: A^0 and $\mathcal{J}$

Three CP odd neutral scalar fields arise from the spontaneous breaking of the electroweak symmetry: one pseudo-scalar Z_L, the longitudinal polarization of the gauge boson Z, one massive pseudo-scalar A^0 and the massless Goldstone mode, associated with the spontaneous breaking of the global symmetry $U(1)_{B-\tilde{L}}$, the Majoron $\mathcal{J}$. [7]

The mass eigenstates are obtained by the basis transformation

$$\begin{pmatrix} a_1 \\ a_2 \\ a_3 \end{pmatrix} = R_{PS} \begin{pmatrix} Z_L \\ \mathcal{J} \\ A^0 \end{pmatrix} , \tag{4.8}$$

where R_{PS} is a 3×3 orthogonal matrix

$$R_{PS} \;=\; \begin{pmatrix} \cos(\beta) & \sin^2(\beta)\,\Delta & -\sin(\beta)\,\tan(\gamma)\,\Delta \\ \sin(\beta) & -\sin(\beta)\,\cos(\beta)\,\Delta & \cos(\beta)\,\tan(\gamma)\,\Delta \\ 0 & \tan(\gamma)\,\Delta & \sin(\beta)\,\Delta \end{pmatrix} , \tag{4.9}$$

with $\Delta = \cos(\gamma)\,/\sqrt{1-\cos(\gamma)^2\cos(\beta)^2}$ and the mixing angles β and γ are by definition

$$\tan(\beta) \;=\; \frac{v_2}{v_1}\,, \qquad\qquad \tan(\gamma) \;=\; \frac{v_3}{v_1}\,. \tag{4.10}$$

The angles β and γ control the coupling of $\mathcal{J}$ to SM fermions. Indeed, the interaction term relevant for the Majoron phenomenology is

$$-\,\mathcal{L} \supset \mathrm{i}\, g_{\mathcal{J}ff}\; \overline{f}\,\gamma_5\, f\,\mathcal{J}\,, \tag{4.11}$$

with

$$g_{\mathcal{J}ff} \;\equiv\; \frac{m_f}{v}\,\sin(\beta)\,\tan(\beta)\,\Delta \tag{4.12}$$

and m_f is the fermion mass. Strong constraints apply on these couplings, stemming from star cooling processes [52]. In particular, the experimental upper limit on the cooling rate of white dwarfs implies: $|g_{\mathcal{J}ee}| \lesssim 10^{-12}$. Then, from (4.10) and (4.12) we obtain in the limit $\beta \ll 1$

$$\beta \lesssim 7 \times 10^{-4} \sqrt{\tan(\gamma)}\,, \tag{4.13}$$

implying $v_2 \lesssim 0.2$ GeV $\sqrt{v_3/v}$. As already stated at the beginning of this section, a hierarchical pattern of the type $v_2 \ll v_3 < v_1$ can be easily fulfilled, as the scale of v_2 is directly related to the dimensional parameter μ':

$$v_2 \;\approx\; \frac{v_1\, v_3\, \mu'}{v_1^2\,\tilde{\kappa}_{12} \,+\, v_3^2\,\kappa_{23} \,-\, 2\,\mu_2^2}\,, \tag{4.14}$$

---

[7] The Majoron $\mathcal{J}$ is exactly massless in our setup. Notice that $\mathcal{J}$, being the Goldstone boson of a spontaneously broken global symmetry, may acquire a mass through gravitational effects, as shown in [50, 51]. However, we will not consider this possibility in the following.

which is suppressed compared to $v_{1,3}$ as μ' can be naturally set to a scale much smaller than the EWSB scale. The second physical pseudo-scalar, A^0, has mass

$$M^2_{A^0} \;=\; \mu' \,\frac{v_2^2(v_1^2+v_3^2)+v_1^2 v_3^2}{2\,v_1 v_2 v_3} \;\sim\; \mu'\,\frac{v_1\,v_3}{2\,v_2} \;=\mu'\,v\,\cos(\beta)\frac{\tan(\gamma)}{2\,\tan(\beta)}. \tag{4.15}$$

The actual value of M_{A^0} depends on the ratio μ'/v_2. Since the couplings of A^0 to the SM fermions are $\sin(\beta)$ suppressed, M_{A^0} and thus μ'/v_2 are unconstrained.

B. Charged scalars: $H^\pm$

As in any two-Higgs doublet model, the charged scalar spectrum is composed of one physical field $H^\pm$ and the eaten longitudinal degree of freedom $W_L^\pm$. They are related to the interaction fields $H_{1,2}$ through the orthogonal transformation:

$$\begin{pmatrix} H_1^+ \\ H_2^+ \end{pmatrix} = \begin{pmatrix} \cos(\beta) & -\sin(\beta) \\ \sin(\beta) & \cos(\beta) \end{pmatrix} \begin{pmatrix} W_L^+ \\ H^+ \end{pmatrix}. \tag{4.16}$$

The charged scalar mass is given by

$$M^2_{H^\pm} = \frac{v^2}{2}\left(\frac{\tan(\gamma)}{\sin(\beta)}\frac{\mu'}{v} - \kappa'_{12}\right) \simeq \frac{M^2_{A^0}}{\cos(\beta)^2} - \frac{v^2}{2}\kappa'_{12}\,, \tag{4.17}$$

where in the last expression we used the approximation given in (4.15). Since $M^2_{H^\pm} > 0$, one requires $\kappa'_{12} \lesssim 2\,M^2_{A^0}/v^2$. An experimental lower bound on $M_{H^\pm}$ is obtained from $H^\pm$ pair production at LEP [53] and the subsequent decays $H^\pm \to \tau^\pm \nu_\tau$ and $H^\pm \to c\,s$. For $m_{H^\pm} \leq m_W$, $H^\pm$ decays only to SM fermions, so the bound $M_{H^\pm} \gtrsim 78.6\,\text{GeV}$ applies.

C. CP even neutral scalars: h^0, H^0 and h_A

We introduce the CP even mass eigenstates h^0, H^0 and h_A, which are related to the interaction fields $h_{1,2,3}$ through the basis rotation:

$$\begin{pmatrix} h_1 \\ h_2 \\ h_3 \end{pmatrix} = R_{NS} \begin{pmatrix} H^0 \\ h_A \\ h^0 \end{pmatrix}, \tag{4.18}$$

In the limit $\mu', v_2 \ll v_3 < v_1$, the CP even scalar mass matrix can be further simplified and R_{NS} just consists in a rotation of angle θ between the eigenstates h^0 and H^0. Moreover, at leading order in β, h_A and the pseudo-scalar A^0 are degenerate in mass and both decouple from the other particles, so no constraints apply on M_{h_A}. Within this approximation and introducing as a shorthand

$$m_1 = v_1\,\sqrt{2\,\lambda_1}\,, \quad m_3 = v_3\,\sqrt{2\,\lambda_3} \quad \text{and} \quad m_{13} = \sqrt{v_1\,v_3\,\kappa_{13}}\,,$$

the masses of the neutral Higgs H^0 and h^0 and the mixing angle θ are given by the relations

$$M^2_{H/h} = \frac{1}{2}\left(m_1^2 + m_3^2 \,\pm\, \sqrt{(m_1^2-m_3^2)^2 \,+\, 4\,m_{13}^4}\right), \quad \theta = \text{Arctan}\left(\frac{m_3^2 - m_1^2 + \sqrt{(m_3^2-m_1^2)^2 \,+\, 4\,m_{13}^4}}{2\,m_{13}^2}\right), \tag{4.19}$$

and $M_{H^0} \geq M_{h^0}$. The mixing angle $|\theta|$ takes values from zero to $\pi/2$. The couplings of H^0 (h^0) to SM particles are given by the SM Higgs ones times $\cos(\theta)$ ($\sin(\theta)$). For maximal $\theta \sim \pi/2$, h^0 couplings are unsuppressed compared to the SM case, so LEP-II bounds apply and $M_{H^0} \geq M_{h^0} \gtrsim 114.4\,\text{GeV}$ [54]. In the opposite case, with suppressed mixing angle $|\theta| \ll 1$, only H^0 get sizable couplings to the SM, and the former bound on M_{H^0} still applies. Conversely, for $|\theta| \ll 1$, LEP-II bounds are rather weak in constraining the mass of the lightest Higgs. Notice that h^0 contributes to the invisible Z decay; however, the $Z - h^0 - J$ coupling is β^4 suppressed: this contribution is negligible and no relevant constraints apply on M_{h^0} from this decay. Nevertheless, for $\sin^2(\theta) \gtrsim 0.1$, LEP-II bounds imply $M_{h^0} \gtrsim 80\,\text{GeV}$. In the following, we assume the conservative limit $M_{h^0} \gtrsim 114.4\,\text{GeV}$, which is valid for all values of θ.

As occurs in models with multiple scalars, the Higgs bosons may decay invisibly. In our scenario, both H^0 and h^0 can decay into two Majorons, thus precluding their detection at present particle colliders, LHC included.

The total decay widths of H^0 and h^0 are given by

$$\Gamma(H/h) \simeq \frac{1}{8\pi} \sum_{ij} \frac{\kappa\left(M_{H/h}, M_i, M_j\right)}{2\, M^3_{H/h}} |\mathcal{M}_{i\,j}|^2\, \Theta\left(M^2_{H/h} - (\,M_i + M_j)^2\right) . \tag{4.20}$$

In the equation given above the kinematical factor is $\kappa(x,y,z) \equiv \sqrt{(x^2-(y+z)^2)(x^2-(y-z)^2)}$. We consider below for simplicity only tree-level two-body decays into identical final states. The decay probabilities of H^0 and h^0 to neutral scalars are proportional to the norms of the trilinear couplings, which at zeroth order in β read:

$$\left|\mathcal{M}^{H/h}_{\mathcal{J}}\right|^2 \;=\; v^2 \left|\lambda^{H/h}_{\mathcal{J}\,\mathcal{J}}\right|^2,\; \lambda^{H/h}_{\mathcal{J}\,\mathcal{J}} = \cos(\beta)\,\kappa_{13} \left\{ \begin{array}{c} \cos(\theta) \\ \sin(\theta) \end{array} \right. - 2\cos(\beta)\tan(\gamma)\,\lambda_3 \left\{ \begin{array}{c} \sin(\theta) \\ -\cos(\theta) \end{array} \right. , \tag{4.21}$$

$$\left|\mathcal{M}^{H/h}_{H^\pm}\right|^2 \;=\; v^2 \left|\lambda^{H/h}_{H^+H^-}\right|^2,\; \lambda^{H/h}_{H^+H^-} = \cos(\beta)\,\kappa_{12} \left\{ \begin{array}{c} \cos(\theta) \\ \sin(\theta) \end{array} \right. - \cos(\beta)\tan(\gamma)\,\kappa_{23} \left\{ \begin{array}{c} \sin(\theta) \\ -\cos(\theta) \end{array} \right. , \tag{4.22}$$

$$\left|\mathcal{M}^{H/h}_{h_A}\right|^2 = \left|\mathcal{M}^{H/h}_{A}\right|^2 \;=\; v^2\, |\lambda^{H/h}_{A\,A}|^2,\; \lambda^{H/h}_{A\,A} = \cos(\beta)\,\tilde{\kappa}_{12} \left\{ \begin{array}{c} \cos(\theta) \\ \sin(\theta) \end{array} \right. - \cos(\beta)\tan(\gamma)\,\kappa_{23} \left\{ \begin{array}{c} \sin(\theta) \\ -\cos(\theta) \end{array} \right. , \tag{4.23}$$

$$\left|\mathcal{M}^{H/h}_{S}\right|^2 \;=\; v^2 \left|\lambda^{H/h}_{S\,S}\right|^2,\; \lambda^{H/h}_{S\,S} = \cos(\beta)\,\mathcal{F}_1 \left\{ \begin{array}{c} \cos(\theta) \\ \sin(\theta) \end{array} \right. - \left(\mathcal{F}_3 \cos(\beta)\tan(\gamma) - \frac{\mu''}{v}\right) \left\{ \begin{array}{c} \sin(\theta) \\ -\cos(\theta) \end{array} \right. \tag{4.24}$$

The decay probabilities of H^0 and h^0 into SM particles are similar to the SM ones, see *e.g.* [55], modulo a dependence on the mixing angles θ and β. At tree level, for the decay probability into fermions, we have

$$\left|\mathcal{M}^{H/h}_{f}\right|^2 \;=\; 2\,N_c \left(\frac{m_f}{v}\right)^2 M^2_{H/h} \left(1 - 4\,\frac{m_f^2}{M^2_{H/h}}\right) \left\{ \begin{array}{c} \cos^2(\theta) \\ \sin^2(\theta) \end{array} \right. , \tag{4.25}$$

where N_c is the number of colors and m_f is the fermion mass. The tree-level $H^0/h^0 \to W^+\,W^-$ decay probabilities depend on

$$\left|\mathcal{M}^{H/h}_{W^\pm}\right|^2 \;=\; \frac{g_W^4}{16}\, v^2 \left|\lambda^{H/h}_{W}(M_{H/h})\right|^2 , \tag{4.26}$$

$$\lambda^{H/h}_{W}(m) \;=\; \cos(\beta)\,\frac{m^2}{M_W^2} \sqrt{1 - 4\frac{M_W^2}{m^2} + 12\,\frac{M_W^4}{m^4}} \left\{ \begin{array}{c} \cos(\theta) \\ \sin(\theta) \end{array} \right. , \tag{4.27}$$

where M_W is the W-boson mass and g_W is the weak gauge coupling constant. A similar expression holds for H^0/h^0 decays into pairs of Z bosons.

From the expressions above, we can estimate the invisible branching ratio of the Higgs bosons. First of all, obviously, the smaller the quartic portal couplings, the smaller the invisible Higgs decay widths. Second, the decays into h_A or A^0, even if equal at leading order in β, do not have a similar impact on Higgs searches at colliders. Indeed, the pseudo-scalar A^0 eventually decays almost exclusively into SM fermions: $H^0/h^0 \to A^0\,A^0$ can thus be considered as a visible channel. Conversely, h_A essentially decays into Majorons.

In the low mass region, $M_{H/h} \lesssim 2\,M_W$, neglecting the masses of the decay products, the Higgs invisible to visible decay width ratios are

$$\frac{\Gamma(H/h \to \text{inv})}{\Gamma(H/h \to \text{SM})} \simeq \frac{\Gamma(H/h \to \mathcal{J}\mathcal{J}) + \Gamma(H/h \to h_A\,h_A) + \Gamma(H/h \to S\,S)}{\Gamma(H/h \to b\,\bar{b}) + \Gamma(H/h \to A^0\,A^0)} , \tag{4.28}$$

provided $M_{h_A} \simeq M_{A^0} \lesssim M_{H/h}/2$. The decay width to b-quarks is Yukawa suppressed, so the ratio above is simplified to

$$\frac{\Gamma(H/h \to \text{inv})}{\Gamma(H/h \to \text{SM})} \simeq 1 + \frac{\Gamma(H/h \to \mathcal{J}\mathcal{J}) + \Gamma(H/h \to S\,S)}{\Gamma(H/h \to A^0\,A^0)} . \tag{4.29}$$

Consequently, for low masses, both H^0 and h^0 mostly decay invisibly.

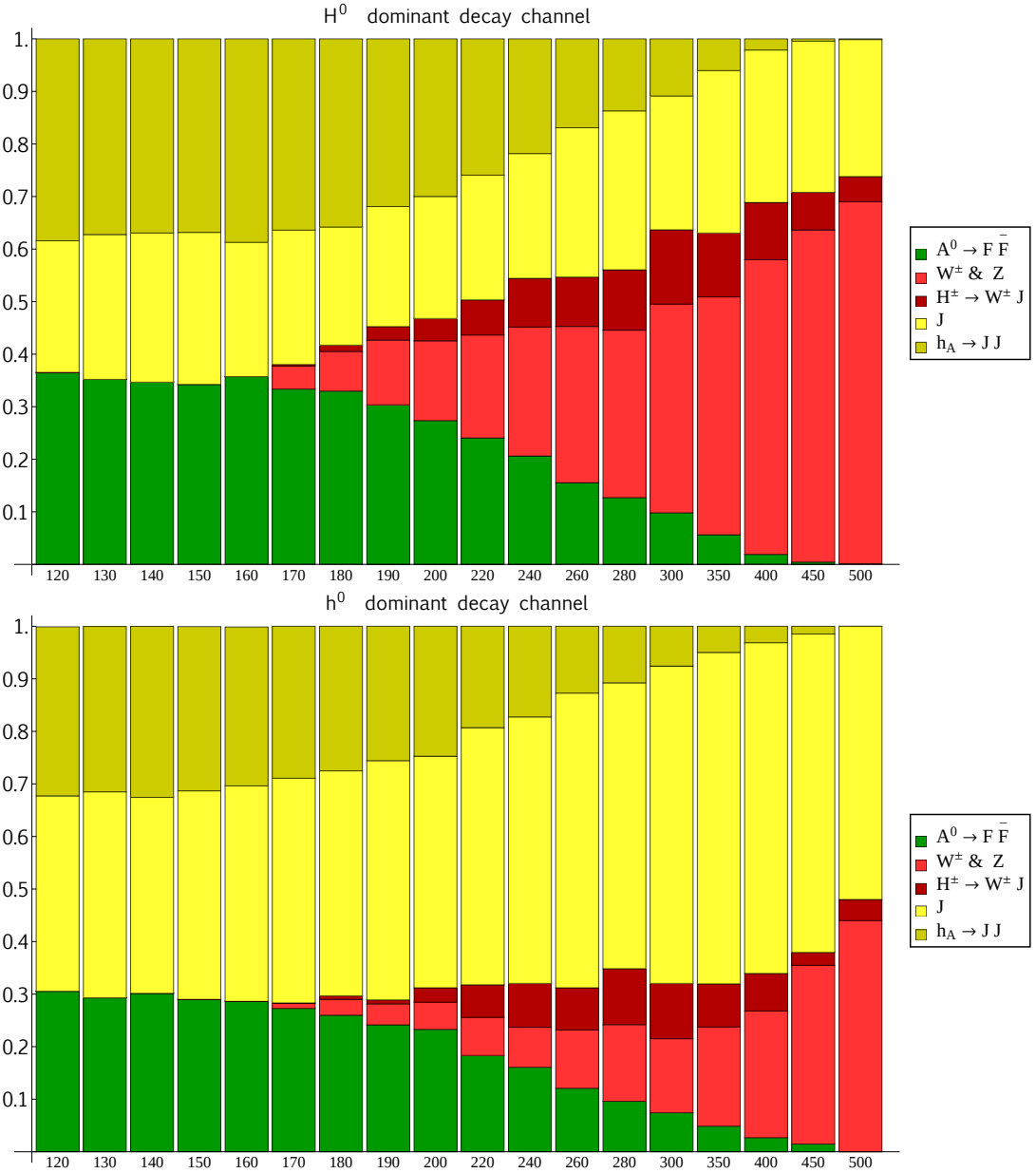

FIG. 11: Dominant H^0 (top) and h^0 (bottom) Higgs decay channels in function of their masses.

In the high mass regime, $M_{H/h} \gtrsim 2\,M_W$, under the approximation that the Majoron channel constitutes the main invisible decay and the visible channel is mostly due to decays to gauge bosons, we have

$$\frac{\Gamma(H/h \to \text{inv})}{\Gamma(H/h \to \text{SM})} \simeq \frac{\Gamma(H/h \to \mathcal{J}\mathcal{J})}{\Gamma(H/h \to W^+W^-) + \Gamma(H/h \to Z\,Z)} \propto \frac{16}{g_W^4}\frac{M_W^4}{M_{H/h}^4}\left(\kappa_{13} \mp 2\,\lambda_3\,\tan(\gamma)\left\{\begin{array}{c}\tan(\theta)\\ 1/\tan(\theta)\end{array}\right.\right)^2 . \quad (4.30)$$

From the previous estimate we infer that, for a maximal $\theta \sim \pi/2$, the heaviest Higgs boson, H^0, decays prevalently into two Majorons, thus forbidding its detection at current collider searches. The opposite occurs for the lightest CP even scalar h^0. On the other hand, for higher values of M_{H^0} (M_{h^0}) and a sufficiently small (large) mixing angle θ, the visible decay rate of H^0 (h^0) becomes sizable. It dominates for very heavy Higgs bosons.

In Fig. 11 we display the frequency at which the H^0 and h^0 decays channels are the dominant ones, displayed in the top and bottom panels, respectively. In order to produce this plot, we use the Higgs decay branching fractions computed by the program micrOMEGAs [56], that we also use to study the Dark Matter sector, as discussed in

Section V. As expected, we see from Fig. 11 that above the W threshold, the heavier the Higgs bosons the larger their visible decay rates. [8] Conversely, in the low mass regime the Higgs bosons are clearly unobservable as we explained above.

V. DARK MATTER

We discuss in this section the third building-block of our model: the existence of a viable Dark Matter candidate. Below the EWSB scale, the complex scalar S is split into two real components S_0 and S_1, the lightest one being the DM. Real scalar singlets provide the simplest DM candidates, for which a large literature exists [57]. In our model, we shall stress two important aspects: first, the stability of DM is not an *ad-hoc* prescription, but results from the remnant $\mathcal{Z}_2$, S_0 or S_1 being the lightest particle odd under this discrete symmetry; second, we emphasize again that introducing the scalar S not only provides a DM candidate, but is also necessary in our leptogenesis scenario.

The masses of the two real components of S are:

$$m^2_{S_{0(1)}} \;=\; \mu_S^2 + \frac{1}{2}\left(\mathcal{F}_1\, v_1^2 + \mathcal{F}_2\, v_2^2 + \mathcal{F}_3\, v_3^2\right) \,\pm\, \left(h\, v_1\, v_2 \,-\, \mu''\, v_3\right) . \tag{5.1}$$

The mass splitting in this case is controlled by the parameters h and μ''. However, since $v_2 \ll v_3$, the latter term dominates and $m_{S^0} \leq m_{S_1}$ for positive μ''. [9]

As seen from $\mathcal{V}_{\rm DM}$, eq. (4.3), S has several portal couplings to the Higgs fields, implying many annihilation channels [58]. Like in most of the singlet scalar DM scenarios, S easily gets a thermal relic abundance in agreement with cosmological requirements.

A. Relic density

The DM annihilation cross-section can generically be written as

$$\sigma\, v \sim \frac{\lambda^2_{eff}}{m_{S^2}}\,, \tag{5.2}$$

where the effective coupling λ_{eff} indicates that each annihilation channel receives in general several contributions. When S annihilates into scalars, the cross-section is the (coherent) sum of the contact term interaction, for which $\lambda_{eff} \propto \mathcal{F}_i$, cf. eq. (4.3), and of scalar-mediated interactions, where λ_{eff} depends on the different trilinear scalar couplings, such as $\lambda^{H/h}_{S\,S}$ introduced in the previous section.

For light DM, that is $m_S \lesssim M_W$, S mostly annihilates to Majorons, as well as to pairs of h_A or A^0, granted the latter are light enough. Notice that the annihilation cross-sections into pairs of h_A and A^0 coincide at zeroth order in β.

For heavier DM, new annihilation channels are open. In the case $m_S > M_W$, S can annihilate into pairs of $W^\pm$ through h^0 and H^0 s-channel (the h_A mediation is β^2 suppressed): [10]

$$\sigma v = \frac{g_W^4}{16\,\pi\, m_S^2}\left(\frac{v^2\,\lambda^H_{S\,S}\,\lambda^H_W(2\,m_S)}{M^2_{H^0} - 4\,m_S^2} + \frac{v^2\,\lambda^h_{S\,S}\,\lambda^h_W(2\,m_S)}{M^2_{h^0} - 4\,m_S^2}\right)^2 , \tag{5.3}$$

where $\lambda^{H/h}_W(m)$ were introduced in eq. (4.27). A similar expression holds for the annihilation into pairs of Z bosons. In the high mass range, S may also annihilate into pairs of charged $H^\pm$, or to pairs of CP even scalars h^0 and H^0.

Increasing the DM mass, the quartic couplings $\mathcal{F}_i$ which control the DM mass, eq. (5.1), and the effective couplings $\lambda^{H/h}_{S\,S}$, eq. (4.24), should increase as well, so that the annihilation cross-section remains large enough, in order to obtain the observed DM relic abundance.

---

[8] Notice that we only consider the two-body decay widths $H^0/h^0 \to W^+\,W^-$. However, in the SM the tree-body decays through off-shell W actually dominate for $M_{H/h} \gtrsim 135\,\text{GeV}$, cf. [55], in which case the Higgs visible decay channels should prevail here as well.

[9] In the following we will however denote by S the DM candidate. The heavier state will decay to DM plus Majoron.

[10] For simplicity, the widths of the Higgs fields have been neglected in eq. (5.3), although they are taken into account in the numerical evaluation.

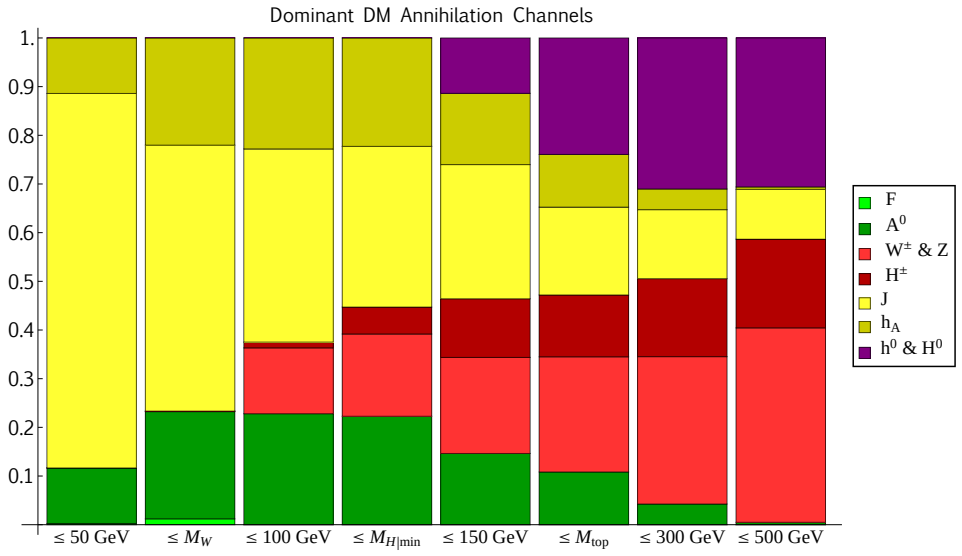

FIG. 12: Main Dark Matter annihilation channels for different Dark Matter mass ranges.

Numerical evaluation

In order to accurately determine the relic abundance of S, we implemented our model in micrOMEGAs [56], through the program FeynRules [40]. We then performed a scan over the full scalar parameter-space, by assigning random values to the different couplings. All λ and κ quartic couplings were varied from 10^{-4} up to the perturbative bound 4π. The trilinear coupling h was chosen between 10^{-6} and 10^{-2}. The scalar masses were randomly varied from their experimental lower bounds, discussed in the previous section, up to 500 GeV. In particular, as regards the CP even scalar masses, recall that we impose the conservative bound $M_{H^0/h^0} \gtrsim 115$ GeV. We vary the mixing angle θ in the range: $0 \leq |\theta| \leq \pi/2$. For the unconstrained scalars h_A and A^0, their (almost degenerate) mass was varied between 1 GeV and 100 GeV.

The trilinear mass term μ'' was scanned over in the range (1-10^2) GeV, while μ' typically took values between 10 eV and 10 MeV. Finally, μ_S was varied from 1 GeV to 500 GeV.

We demand the relic density of S to account for all the DM abundance and to lie within the 3σ range of WMAP [16]:

$$\Omega_{\rm DM} = 0.229 \pm 0.045\,.$$

We illustrate the relative contributions of the different annihilation channels in Fig. 12. Binning the DM mass range into intervals of interest, we present the frequency at which a given channel is the dominant one. For example, before the W channel is kinematically open, *i.e.* for $m_S \leq M_W$, we see from Fig. 12 that S annihilates only into pairs of $\mathcal{J}$, A^0 and h_A. For heavier DM mass, new annihilation processes are possible. In particular, annihilation into gauge bosons, charged scalars or CP even scalars tend to be the dominant processes. Notice that Fig. 12 only displays the frequency a given annihilation channel dominates in a given mass interval and not the relative contributions of the different channels.

B. Direct detection constraints

The Dark Matter can scatter on nucleons through scalar-mediated t-channels: the spin-independent (SI) elastic cross-section receives contributions from both h^0 and H^0 exchange, according to:

$$\sigma_n^{SI} = \frac{1}{4\pi}\frac{\mu_{S,n}^2}{m_{S_0}^2}\, m_n^2\, f_n^2 \left(\frac{\lambda_{H^0}}{M_{H^0}^2} + \frac{\lambda_{h^0}}{M_{h^0}^2}\right)^2 . \tag{5.4}$$

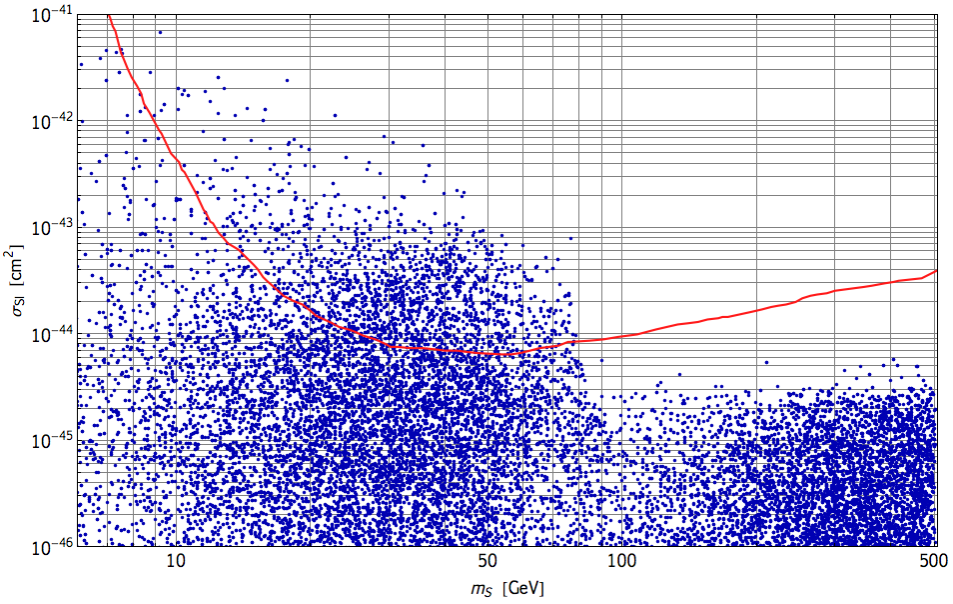

FIG. 13: Spin-independent cross-section against m_S: the blue points are the model predictions which provide the required relic density. The red line represents XENON100 results, extracted from [21].

In this expression, $\mu_{S,n}$ is the S-nucleon reduced-mass and m_n the nucleon mass. The factor f_n is the effective Higgs-nucleon interaction and varies from 0.14 to 0.66 [59]. The couplings λ_{H^0} and λ_{h^0} are given by

$$\lambda_{H/h} = \frac{1}{\cos(\beta)}\,\lambda_{SS}^{H/h}\,\begin{cases}\cos(\theta)\\ \sin(\theta)\end{cases} \tag{5.5}$$

Assuming the conservative bound $M_{H^0/h^0} \gtrsim 115$ GeV, we see from the previous expression that for $\theta \approx 0$ $(\pi/2)$ the main contribution comes from H^0 (h^0) exchange and σ_n^{SI} is then mostly affected by $\mathcal{F}_1$. Notice that, contrary to [60], where the mixing suppression $\theta \ll 1$ was balanced by a very light scalar h^0 ($M_{h^0} \lesssim 1\,\text{GeV}$), in the present scenario, taking M_{h^0} above the LEP-II bound drastically forbids such an enhancement. In the limit of small mixing angle θ, assuming $f_n \sim 1/3$, the SI elastic cross-section can be roughly expressed as

$$\sigma_n^{SI} \simeq \frac{1}{\pi}\frac{m_n^4}{m_S^2}\,f_n^2\left(\frac{\mathcal{F}_1}{M_{H^0}^2}\right)^2 \sim 6\times 10^{-44}\,\text{cm}^2\left(\frac{m_S}{100\,\text{GeV}}\right)^{-2}\left(\frac{M_{H^0}}{120\,\text{GeV}}\right)^{-4}\left(\frac{\mathcal{F}_1}{0.1}\right)^2, \tag{5.6}$$

which shows that S can easily saturate current direct-detection bound for electroweak scale DM [18]-[21]. As we saw in the previous subsection, since the annihilation cross-section scales as $(\mathcal{F}_k/m_S)^2$, the couplings $\mathcal{F}_k$ should be sizable for large DM masses, otherwise S relic density would overclose the Universe. This, in turn, implies that for heavy DM the scattering cross-section on nucleons is almost independent of the DM mass, cf. eq. (5.5).

The dependence of σ_n^{SI} on m_S in the low and high DM mass regimes is manifest in Fig. 13. In this plot we compare the model predictions (blue dots) for σ_n^{SI} with XENON100 results [21] (red curve). We can see that while only a small region of the parameter-space is already excluded by current data, the next generation of direct-detection experiments would probe a large part of it [61]. Notice in particular that in the low mass regime high cross-sections can be reached, due to non-suppressed $\mathcal{F}_{1,3}$ couplings. A light DM with large $\mathcal{F}_{1,3}$ couplings is possible through a partial cancellation in eq. (5.1), which depends on the value of the parameter μ''.

VI. CONCLUSIONS

In this paper we study a seesaw extension of the Standard Model based on a global $U(1)_{B-\tilde{L}}$ symmetry group, where $\tilde{L}$ can be thought as a generalized lepton charge. This global symmetry is spontaneously broken at the electroweak scale. Suitable scalar and fermion representations are added to the SM particle content so that a tiny Majorana mass for active neutrinos is naturally generated, in agreement with neutrino oscillation experiments. More specifically, an

extra Higgs doublet H_2 and a Higgs singlet H_3 are added to the SM, together with a heavy Dirac fermion N_D. The lepton doublets and N_D interact through neutrino Yukawa couplings which can violate the lepton number. When N_D mass is set at the TeV scale, the model realizes a UV-completion of the inverse-seesaw mechanism.

We show that, with the addition of two extra SM-singlets in the model, a Majorana fermion N_3 and a complex scalar S, it is possible to explain quantitatively both the observed baryon asymmetry of the Universe through an original leptogenesis mechanism and the Dark Matter relic abundance.

Leptogenesis in this model is implemented in two steps: first an asymmetry in N_D and S is generated by the out-of-equilibrium decays of N_3. In a second step this asymmetry is converted in a non-zero lepton charge due to fast neutrino Yukawa interactions. The latter constitute a link between leptogenesis and neutrino mass generation. We solve numerically the Boltzmann equations relevant for this two-step leptogenesis scenario and show that the observed amount of baryon asymmetry is easily achieved. We concentrate the discussion on a TeV scale scenario, and show that, provided neutrino mass constraints are fulfilled, no lower-bound on the mass of N_D is imposed by the requirement of a successful leptogenesis. However, this scenario of leptogenesis is also viable at much larger scales. An important feature of this mechanism is that the source and damping terms do not depend on the same couplings, therefore large CP asymmetries can be obtained even in the regime of weak washouts.

In the second part of the paper, we analyze in detail the mass spectrum of the model and provide constraints on the parameter-space arising from low-energy physics. In particular, we show that the presence of a massless Majoron, which corresponds to the Goldstone boson associated with the spontaneous breaking of the global $U(1)_{B-\tilde{L}}$ symmetry, has an important impact on Higgs boson searches. Indeed, light Higgs scalars H^0 and h^0, $M_{H^0/h^0} \lesssim 140$ GeV, would mainly decay into pairs of Majorons, thus making difficult their observation at colliders, LHC included.

Concerning the scalar field S, after the breaking of the electroweak symmetry, the lightest component of S remains stable, due to the presence of a remnant $\mathcal{Z}_2$ symmetry, and provides a viable candidate for Dark Matter. Its mass is unconstrained and can take values as light as few GeV up to few TeV. Numerous annihilation channels are present, allowing the relic DM density to be consistent with cosmological observations. We study the possible signatures of DM in direct detection experiments, and show that while the current constraints exclude already a part of the parameter-space, a large region may be probed by the next generation of detectors.

This model explains in a common framework three main experimental issues: neutrino mass generation, the baryon asymmetry of the Universe and the Dark Matter relic density. Many observables are predicted, but their measurements probe uncorrelated sectors, making this minimal extension difficult to falsify.

Acknowledgements

The authors acknowledge N. Bernal for early stage discussions and S. Palomares-Ruiz for useful comments. The work of F.X.J.M. and E.M. is supported by Fundação para a Ciência e a Tecnologia (FCT, Portugal) through the projects PTDC/FIS/098188/2008, CERN/FP/116328/2010 and CFTP-FCT Unit 777, which are partially funded through POCTI (FEDER).

Appendix A: Interaction Lagrangian of the Model

The full interaction Lagrangian of the model is:

$$\begin{aligned}\mathcal{L}_{\rm int} &= \mathcal{L}_{\rm int}^{\rm SM} - \mathcal{V}_{\rm SB} - \mathcal{V}_{\rm DM} - M\,\overline{N}_D N_D - \frac{1}{2} M_3\,\overline{N}_3\,N_3^c \\ &\quad - \left(y_1^i\,\overline{N}_D\,\widetilde{H}_1^\dagger\,\ell_i + y_2^j\,\overline{N}_D^c\,\widetilde{H}_2^\dagger\,\ell_j + \frac{\alpha}{\sqrt{2}}\,H_3\,\overline{N}_D\,N_D^c + g\,S\,\overline{N}_D\,N_3 + \text{h.c.}\right), \end{aligned} \tag{A1}$$

where $\mathcal{L}_{\rm int}^{\rm SM}$ is the Yukawa interaction Lagrangian of the Standard Model and

$$\begin{aligned}\mathcal{V}_{\rm SB} &= -\mu_1^2\,H_1^\dagger H_1 + \lambda_1\,(H_1^\dagger H_1)^2 - \mu_2^2\,H_2^\dagger H_2 + \lambda_2\,(H_2^\dagger H_2)^2 - \mu_3^2\,H_3^* H_3 + \lambda_3\,(H_3^* H_3)^2 \\ &\quad + \kappa_{12}\,H_1^\dagger H_1 H_2^\dagger H_2 + \kappa'_{12}\,H_1^\dagger H_2 H_2^\dagger H_1 + \kappa_{13}\,H_1^\dagger H_1 H_3^* H_3 + \kappa_{23}\,H_2^\dagger H_2 H_3^* H_3 \\ &\quad - \frac{\mu'}{\sqrt{2}}\left(H_1^\dagger H_2 H_3 + H_2^\dagger H_1 H_3^*\right), \end{aligned} \tag{A2}$$

$$\begin{aligned}\mathcal{V}_{\rm DM} &= \mu_S^2\,S^*S + \lambda_S\,(S^*S)^2 + \mathcal{F}_1\,H_1^\dagger H_1 S^*S + \mathcal{F}_2\,H_2^\dagger H_2 S^*S + \mathcal{F}_3\,H_3^* H_3 S^*S \\ &\quad + h\,S^2 H_1^\dagger H_2 + h^*\,S^{*2} H_2^\dagger H_1 - \frac{\mu''}{\sqrt{2}}(S^2 H_3^* + S^{*2} H_3)\,. \end{aligned} \tag{A3}$$

Appendix B: Computation of the CP Asymmetry

The relevant interaction Lagrangian which is involved in the generation of the CP asymmetry in the out-of-equilibrium decays of the Majorana neutrino N_3 is the following:

$$-\mathcal{L}_{int} \supset \frac{\alpha}{\sqrt{2}} H_3 \overline{N}_D N_D^c + g S \overline{N}_D N_3 - \frac{\mu''}{\sqrt{2}} S^2 H_3^* + \text{h.c.},$$

where $N_D^c \equiv C\overline{N}_D^T$, $N_3 \equiv N_3^c \equiv C\overline{N}_3^T$. The CP asymmetry in the decays of N_3 is defined as:

$$\begin{aligned} \epsilon_{CP} &\equiv -\frac{\Gamma\left(N_3 \to \overline{N}_D + S\right) - \Gamma\left(N_3 \to N_D + \overline{S}\right)}{\Gamma\left(N_3 \to \overline{N}_D + S\right) + \Gamma\left(N_3 \to N_D + \overline{S}\right)} \\ &= -\frac{\text{Im}\left\{\int d\tilde{\Pi}_{N,S}\, \mathcal{M}^{(0)}(N_3 \to \overline{N}_D\, S)^* \sum\limits_{\{n\}} \int d\tilde{\Pi}_{\{n\}}\, \mathcal{M}^{(0)}(N_3 \to \{n\})\, \mathcal{M}^{(0)}(\{n\} \to \overline{N}_D\, S)\right\}}{\int d\tilde{\Pi}_{N,S} \left|\mathcal{M}^{(0)}(N_3 \to \overline{N}_D\, S)\right|^2}, \end{aligned} \tag{B1}$$

where $\sum_{\{n\}}$ indicates the sum over all possible on-shell states in the loop of Fig. 1, while the phase space factor in the integral is, in general

$$d\tilde{\Pi}_{n_1,\ldots,n_k} \equiv \frac{d^3 p_{n_1}}{(2\pi)^3 2E_{n_1}} \cdot \ldots \cdot \frac{d^3 p_{n_k}}{(2\pi)^3 2E_{n_k}} (2\pi)^4 \delta^{(4)}\left(p_{N_3} - \sum_{j=1}^{k} p_{n_j}\right), \qquad k \geq 2\,, \tag{B2}$$

p_{N_3} and p_{n_j} $(j = 1, \ldots, k)$ being the 4-momenta of the decaying Majorana neutrino N_3 and the final state n_j, respectively. We consider the physical intermediate processes: [11] $N_3 \to N_D + \overline{S}$ and $N_D + \overline{S} \to \overline{N}_D + S$. The corresponding tree-level amplitudes read: [12]

$$\begin{aligned} i\mathcal{M}^{(0)}(N_3 \to \overline{N}_D + S) &= ig\, v_N^T(\mathbf{p}_N)\, C^{-1}\, u_{N_3}(\mathbf{p}_{N_3}), \\ i\mathcal{M}^{(0)}(N_3 \to N_D + \overline{S}) &= -ig\, \overline{u}_N(\mathbf{p}'_N)\, u_{N_3}(\mathbf{p}_{N_3}), \\ i\mathcal{M}^{(0)}(N_D + \overline{S} \to \overline{N}_D + S) &= -\frac{i}{p^2_{H_3} - m_3^2} \frac{\mu''}{2} \left(\alpha^*\, v_N^T(\mathbf{p}_N)\, C^{-1}\, u_N(\mathbf{p}'_N)\right). \end{aligned} \tag{B3}$$

We perform the product of the three amplitudes in (B3) according to eq. (B1) and sum over the polarizations of the outgoing fermions. After some algebra, we get

$$\mathcal{M}^{(0)}(N_3 \to \overline{N}_D + S)^*\, \mathcal{M}^{(0)}(N_3 \to N_D + \overline{S})\, \mathcal{M}^{(0)}(N_D + \overline{S} \to \overline{N}_D + S) =$$

$$2\, g^2\, \alpha^*\, \frac{\mu'' M^2 M_3}{p^2_{H_3} - m_3^2} \left[1 + \frac{(p_N \cdot p'_N)}{M^2} + \frac{((p_N + p'_N) \cdot p_{N_3})}{M M_3}\right].$$

Integration over the phase space

The relevant integrals in the numerator of (B1) are

$$I_n = \int \frac{d^3 p'_N}{(2\pi)^3 2E'_N} \frac{d^3 p'_S}{(2\pi)^3 2E'_S} \frac{S_n}{p^2_{H_3} - m_3^2} (2\pi)^4 \delta^{(4)}\left(p_{N_3} - p'_N - E'_S\right), \tag{B4}$$

where $S_n \in \{(p_N \cdot p'_N),\, (p'_N \cdot p_{N_3}),\, (p_N \cdot p_{N_3}),\, M^2\}$.

---

[11] Notice that the other possible cuts in Fig. 1 do not contribute to the CP asymmetry as they do not correspond to physical processes.

[12] In the following we indicate with m_3 the thermal mass of the scalar singlet H_3, which provides an infrared regulator of the the N_3 decay one-loop diagram.

It is convenient to express I_n in terms of adimensional quantities, mainly: $a \equiv E_N/M_3$, $b \equiv |\mathbf{p}_N|/M_3$, $x \equiv M/M_3$, $x_S \equiv m_S/M_3$ and $x_3 \equiv m_3/M_3$:

$$I_1 = \frac{1}{32\pi}\left[-2\,\kappa(1,x,x_S) + \frac{2x^2 - x_3^2}{b}\,C\left(x, x_S, x_3, a, b\right)\right], \tag{B5}$$

$$I_{2,3,4} = \frac{1}{32\pi}\frac{1}{b}\left\{B(x,x_S), 2a, 2x^2\right\}\,C\left(x, x_S, x_3, a, b\right), \tag{B6}$$

where κ is a kinematic factor introduced below eq. (4.20), $B(s,t) = \sqrt{\kappa\left(1,s,t\right)^2 + 4s^2}$ and

$$C\left(s,t,u,a,b\right) = \log\left(\frac{2s^2 - u^2 - a\,B\left(s,t\right) + b\,\kappa\left(1,t,s\right)}{2s^2 - u^2 - a\,B\left(s,t\right) - b\,\kappa\left(1,t,s\right)}\right). \tag{B7}$$

Now we complete the integration over the phase space in the numerator of eq. (B1). The relevant integrals can be arranged in the form:

$$J_n = \frac{1}{4\pi}\int_0^\infty da \frac{\sqrt{a^2 - x^2}}{1-a}\,I_n\,\delta\left(1 - a - \sqrt{a^2 - x^2 + x_S^2}\right). \tag{B8}$$

The full computation results in:

$$J_1 = \frac{1}{128\pi^2}\left[-\kappa\left(1,x,x_S\right)^2 + (2x^2 - x_3^2)\log\left(\frac{x_3^2}{x_3^2 + \kappa\left(1,x,x_S\right)^2}\right)\right], \tag{B9}$$

$$J_2 = J_3 = \frac{1}{128\pi^2}\,B\left(x,x_S\right)\log\left(\frac{x_3^2}{x_3^2 + \kappa\left(1,x,x_S\right)^2}\right), \tag{B10}$$

$$J_4 = \frac{1}{64\pi^2}\,x^2\log\left(\frac{x_3^2}{x_3^2 + \kappa\left(1,x,x_S\right)^2}\right). \tag{B11}$$

A similar computation applies for the denominator of eq. (B1). We have in this case:

$$\int d\tilde{\Pi}_{N,S}\left|\mathcal{M}^{(0)}(N_3 \to \overline{N}\,S)\right|^2 = g^2\,\frac{M_3^2}{4\pi}\kappa\left(1,x,x_S\right)\left[2x + B\left(x,x_S\right)\right]. \tag{B12}$$

The CP asymmetry in the decays

Taking into account the results obtained in eqs. (B9)-(B12) and the general expression (B1), we get the final expression of the CP asymmetry:

$$\epsilon_{CP} = -\frac{1}{16\pi}\,\frac{\mu''}{M_3}\,\mathrm{Im}(\alpha)\,\frac{F_2(x,x_S,x_3) + 2x\,\left[x + B\left(x,x_S\right)\right]F_1(x,x_S,x_3)}{2x + B\left(x,x_S\right)}, \tag{B13}$$

where

$$F_1(x,x_S,x_3) = \frac{1}{\kappa\left(1,x,x_S\right)}\log\left(\frac{x_3^2}{x_3^2 + \kappa\left(1,x,x_S\right)^2}\right), \tag{B14}$$

$$F_2(x,x_S,x_3) = -\kappa\left(1,x,x_S\right) + (2x^2 - x_3^2)F_1(x,x_S,x_3). \tag{B15}$$

Therefore in the limit $m_S,\, M \ll M_3$, which we are interested in, we get the approximation reported in eq. (3.2):

$$\epsilon_{CP} \simeq -\frac{1}{16\pi}\,\frac{\mu''}{M_3}\,\mathrm{Im}(\alpha).$$

Appendix C: Boltzmann Equations

In this appendix, we introduce the set of Boltzmann Equations (BE) that are used for the numerical evaluation of the baryon asymmetry. More details on the network of BE can be found in the appendices of [35] and [44]. For a given particle (asymmetry) X, we denote as usual by Y_X its comoving number density, *i.e.* the number density normalized to the entropy density. We assume Maxwell-Boltzmann statistics for both fermions and scalars. In an expanding Universe, the evolution of Y_X is governed by the Boltzmann equation:

$$s\,H(z)\frac{dY_X}{dz} \;= -\sum_{a,i,j,\,\ldots}\,[X\,a\;\rightleftarrows\,i\,j\,]\;,$$

where

$$[X\,a\;\rightleftarrows\,i\,j\,]\equiv\frac{Y_X}{Y_X^{eq}}\frac{Y_a}{Y_a^{eq}}\,\gamma^{eq}(X\,a\to i\,j)-\frac{Y_i}{Y_i^{eq}}\frac{Y_j}{Y_j^{eq}}\,\gamma^{eq}(i\,j\to X\,a)\,,$$

and $z=M_3/T$ is the evolution parameter, while γ^{eq} are the equilibrium reaction densities of the different processes. We will limit our analysis to $1\leftrightarrow 2$ and $2\leftrightarrow 2$ processes, but will include the on-shell part of some $2\leftrightarrow 3$ scatterings for consistency. If these processes conserve CP, then we use the notation $[X\,a\leftrightarrow i\,j]$, as $\gamma^{eq}(X\,a\to i\,j)=\gamma^{eq}(i\,j\to X\,a)$.

In a radiation dominated Universe, the Hubble constant $H(T)$ and the entropy density s are given by

$$H(T)\;=\;\sqrt{\frac{4\,\pi^3\,g_*}{45}}\frac{T^2}{M_{\rm pl}}\,,\quad s=g_*\,\frac{2\,\pi^2}{45}\,T^3\,.$$

In these equations, g_* is the number of relativistic degrees of freedom present in the thermal bath at the leptogenesis time scale. In the case of the SM, at temperatures above the EWSB, one has $g_*^{\rm SM}=106.75$. Assuming that the non-SM scalars S, H_2 and H_3 and the Dirac fermion N_D are relativistic particles at $T\approx M_3$, we obtain: $g_*=g_*^{\rm SM}+46/4=118.25$.

As already explained in Section III, the main source of N_D and S asymmetry production during the first stage of leptogenesis are the CP-violating decays and inverse decays of N_3,

$$\gamma^{eq}\left(N_3\rightleftarrows N_D\,\overline{S}\right)\equiv\gamma_D\left(\frac{1\pm\epsilon_{CP}}{2}\right)=\gamma^{eq}\left(N_3\leftrightarrows\overline{N}_D\,S\right)\,,$$

where ϵ_{CP} is the CP asymmetry in the decays, defined in eq. (B1), and γ_D is the CP conserving total decay width of N_3. The last equality results from CPT invariance.

We further include in the BE $\Delta N_D=\Delta S=2$ scatterings shown in Fig. 2, whose corresponding collision rates are denoted as:

$$\gamma^{eq}(N_D\,\overline{S}\rightleftarrows\overline{N}_D\,S)\equiv\gamma^a_{\Delta 2}\quad\text{and}\quad\gamma^{eq}(N_D\,N_D\leftrightarrow S\,S)\equiv\gamma^b_{\Delta 2}\,.$$

Note that, as in standard leptogenesis, $N_D\,\overline{S}\rightleftarrows\overline{N}_D\,S$ processes mediated by N_3 in a s-channel develop an on-shell part, which is CP-violating. To avoid double-counting of this resonant part, already accounted for by the inverse decays, the on-shell contribution should be subtracted from the full $N_D\,\overline{S}\leftrightarrow\overline{N}_D\,S$ scattering rate.

In addition to the standard source term given by the decays of N_3, we include the CP violation arising from the $2\leftrightarrow 2$ scatterings involving an external N_3, which also depends on the CP-violating phase α entering in ϵ_{CP}, eq. (3.2). The CP asymmetry for each diagram is computed as in the standard leptogenesis scenario, *e.g.* [62] and [63]. However, in our model a contribution to CP asymmetry in the N_3-scatterings arises from both s-, t- and u-channels, as depicted in Fig. 3. The corresponding thermal rates, in this case, are:

a) $\gamma^{eq}(N_D\;N_3\rightleftarrows H_3\;\overline{S})\;\equiv\;\gamma^a_{N_3}\,(1\pm\epsilon^a_{CP})\;=\;\gamma^{eq}(\overline{N}_D\;N_3\leftrightarrows\overline{H}_3\;S)\,.$

b) $\gamma^{eq}(N_3\;S\rightleftarrows\overline{N}_D\;H_3)\equiv\gamma^b_{N_3}\left(1\mp\epsilon^b_{CP}\right)\;=\;\gamma^{eq}(N_3\;\overline{S}\leftrightarrows N_D\;\overline{H}_3)\,.$

c) $\gamma^{eq}(N_D\;S\rightleftarrows N_3\;H_3)\;\equiv\;\gamma^c_{N_3}\,(1\mp\epsilon^c_{CP})\;=\gamma^{eq}(\overline{N}_D\;\overline{S}\leftrightarrows N_3\;\overline{H}_3)\,.$

d) $\gamma(N_3\;S\rightleftarrows H_1\;\ell)\;\equiv\;\gamma^d_{N_3}\,(1\pm\epsilon_{CP})\;=\gamma(N_3\;\overline{S}\leftrightarrows\overline{H}_1\;\overline{\ell})\,.$

e) $\gamma(N_3\;S\rightleftarrows\overline{H}_2\;\overline{\ell})\;\equiv\;\gamma^e_{N_3}\,(1\pm\epsilon_{CP})\;=\gamma(N_3\;S\leftrightarrows H_2\;\ell)\,.$

The CP asymmetries in the scattering, ϵ^k_{CP} ($k = a, ..., e$), are defined by $\epsilon^k_{CP} \equiv \epsilon_{CP}\, \Delta K^k$, with

$$\Delta K^{a,b} \equiv \frac{\left(\gamma^{a,b}_{N_3}\right)_t - \left(\gamma^{a,b}_{N_3}\right)_s}{\gamma^{a,b}_{N_3}}\,, \quad \Delta K^c \equiv \frac{\left(\gamma^c_{N_3}\right)_t - \left(\gamma^c_{N_3}\right)_u}{\gamma^c_{N_3}}\,, \quad \Delta K^d = \Delta K^e = 1\,.$$

Here $\left(\gamma^k_{N_3}\right)_c$, $c = (s, t, u)$, corresponds to the s-, t- and u-channels of the different processes shown in Fig. 3. Notice that, similarly to the $\Delta N_D = \Delta S = 2$ scatterings considered before, as explained in [63], we have to subtract the resonant CP-violating contribution of the $2 \leftrightarrow 3$ processes in which N_3 is exchanged in s-channel. The non-resonant parts of such processes are not taken into account in our computation, since they are at higher order in the couplings.

As regards N_3 three-body decays, which are at the same order in the couplings as $2 \leftrightarrow 2$ scatterings on N_3, they are phase-space suppressed and so give a sub-leading contribution with respect to the two-body decays [63], and we consequently do not include them.

We further consider the effect of S self-annihilations (see Fig. 4), which could washout the asymmetry $Y_{\Delta S}$ for large values of the coupling h (see eq. (4.3)). The related interaction density rate is noted

$$\gamma^{eq}(S\,S \,\leftrightarrow\, H_1\,\overline{H}_2) \equiv \gamma_{SS}\,.$$

Several processes participate in the second phase of leptogenesis. Besides the scatterings on N_3, the $\gamma^{d,e}_{N_3}$ discussed above, we include the following interactions, at the lowest order in the neutrino Yukawa couplings:

a) N_D decays and inverse decays: $\gamma^{eq}(N_D \,\leftrightarrow\, \ell_\alpha\, H_1) \equiv \gamma_{D\ell}$ and $\gamma^{eq}(N_D \,\leftrightarrow\, \overline{\ell_\beta}\,\overline{H}_2) \equiv \gamma_{D\bar{\ell}}$.

b) $\Delta L = 1$, H_1-mediated scatterings with top-quark: $\gamma^{eq}(N_D\overline{\ell} \leftrightarrow Q_3\,\bar{t}) \equiv \gamma^s_{N_D}$ for the s-channel contribution and $\gamma^{eq}(N_D q_3 \leftrightarrow \ell\, t) + \gamma^{eq}(N_D\bar{t} \leftrightarrow \ell\,\overline{q_3}) = 2\,\gamma^t_{N_D}$ for the t-channel contributions.

As already stated in Section III, the leptons participate in N_D mediated $\Delta L = 2$ scatterings: $\gamma^a_{\ell\ell} \equiv \gamma^{eq}(\ell\, H_1 \leftrightarrow \overline{\ell}\,\overline{H}_2)$ and $\gamma^b_{\ell\ell} \equiv \gamma^{eq}(\ell\,\ell \leftrightarrow \overline{H}_1\,\overline{H}_2)$.

We are ready now to report the complete set of Boltzmann equations relevant for the computation of the baryon asymmetry of the Universe in the two-step leptogenesis scenario described in the text. We include all the interaction terms introduced above and we use the simplified notation $y_{N_3} \equiv Y_{N_3}/Y^{eq}_{N_3}$, $y_{\Delta X} \equiv Y_{\Delta X}/Y^{eq}_X$ and $Y'_X \equiv (s\,H(z))\,dY_X/dz$. At first order in the asymmetry (zeroth order for N_3), the full system of Boltzmann equations is the following:

$$\begin{aligned}
Y'_{N_3} \;=\;& -\left[N_3 \rightleftarrows N_D\,\overline{S}\right] - \left[N_3 \rightleftarrows \overline{N}_D\,S\right] - \left[N_D\,N_3 \rightleftarrows H_3\,\overline{S}\right] - \left[\overline{N}_D\,N_3 \rightleftarrows \overline{H}_3\,S\right] \\
&- \left[S\,N_3 \rightleftarrows \overline{N}_D\,H_3\right] - \left[\overline{S}\,N_3 \rightleftarrows N_D\,\overline{H}_3\right] + \left[S\,N_D \rightleftarrows N_3\,H_3\right] + \left[\overline{S}\,\overline{N}_D \rightleftarrows N_3\,\overline{H}_3\right] \\
&+ \left[\ell\,H_1 \rightleftarrows N_3\,S\right] + \left[\overline{\ell}\,\overline{H}_1 \rightleftarrows N_3\,\overline{S}\right] + \left[H_2\,\ell \rightleftarrows N_3\,\overline{S}\right] + \left[\overline{H}_2\,\overline{\ell} \rightleftarrows N_3\,S\right]\,,
\end{aligned}$$

$$\begin{aligned}
Y'_{N_D} \;=\;& \left[N_3 \rightleftarrows N_D\,\overline{S}\right] - \left[N_D\,\overline{S} \rightleftarrows \overline{N}_D\,S\right] - \left[N_D\,N_D \leftrightarrow S\,S\right] \\
&- \left[N_D\,N_3 \rightleftarrows H_3\,\overline{S}\right] - \left[N_D\,\overline{H}_3 \rightleftarrows N_3\,\overline{S}\right] - \left[N_D\,\overline{S} \rightleftarrows N_3\,H_3\right] \\
&- \left[N_D \leftrightarrow \ell H_1\right] - \left[N_D \leftrightarrow \overline{\ell}\,\overline{H}_2\right] - \left[N_D\,\overline{\ell} \leftrightarrow q_3\,\bar{t}\right] - \left[N_D\,q_3 \leftrightarrow \ell\,t\right] - \left[N_D\,\bar{t} \leftrightarrow \ell\,\overline{q_3}\right]\,,
\end{aligned}$$

$$\begin{aligned}
Y'_S \;=\;& \left[N_3 \leftrightarrows S\,\overline{N}_D\right] - \left[S\,\overline{N}_D \rightleftarrows \overline{S}\,N_D\right] - \left[S\,S \,\leftrightarrow N_D\,N_D\right] \\
&- \left[S\,\overline{H}_3 \rightleftarrows N_3\,N_D\right] - \left[S\,N_3 \rightleftarrows \overline{N}_D\,H_3\right] - \left[S\,N_D \rightleftarrows N_3\,H_3\right] \\
&- \left[S\,N_3 \rightleftarrows \ell H_1\right] - \left[S\,N_3 \rightleftarrows \overline{\ell}\,\overline{H}_2\right] - \left[S\,S \leftrightarrow H_1\,\overline{H}_2\right]\,,
\end{aligned}$$

$$\begin{aligned}
Y'_\ell \;=\;& \left[N_D \leftrightarrow \ell H_1\right] + \left[\overline{N}_D \leftrightarrow \ell H_2\right] - \left[\ell\,\overline{N}_D \leftrightarrow \overline{q_3}\,t\right] - \left[\ell\,t \leftrightarrow N_D\,q_3\right] - \left[\ell\,\overline{q_3} \leftrightarrow N_D\,\bar{t}\right] \\
&- \left[\ell\,H_1 \rightleftarrows N_3\,S\right] - \left[\ell\,H_2 \rightleftarrows N_3\,\overline{S}\right] - \left[\ell\,H_1 \leftrightarrow \overline{\ell}\,\overline{H}_2\right] - \left[\ell\,\ell \leftrightarrow \overline{H}_1\,\overline{H}_2\right]\,,
\end{aligned}$$

$$Y'_{H_1} \;=\; \left[N_D \leftrightarrow H_1\,\ell\right] - \left[H_1\,\ell \rightleftarrows N_3\,S\right] - \left[H_1\,\overline{H}_2 \leftrightarrow\, S\,S\right] - \left[\ell\,H_1 \leftrightarrow \overline{\ell}\,\overline{H}_2\right] - \left[H_1\,H_2 \leftrightarrow \overline{\ell}\,\overline{\ell}\right]\,,$$

$$Y'_{H_2} \;=\; \left[N_D \leftrightarrow \ell\,H_2\right] - \left[H_2\,\ell \rightleftarrows N_3\,\overline{S}\right] - \left[H_2\,\overline{H}_1 \leftrightarrow\, \overline{S}\,\overline{S}\right] - \left[\ell\,H_2 \leftrightarrow \overline{\ell}\,\overline{H}_1\right] - \left[H_1\,H_2 \leftrightarrow \overline{\ell}\,\overline{\ell}\right]\,,$$

$$Y'_{H_3} \;=\; -\left[H_3\,\overline{S} \rightleftarrows N_3\,N_D\right] - \left[H_3\,\overline{N}_D \rightleftarrows N_3\,S\right] - \left[H_3\,N_3 \rightleftarrows N_D\,S\right] .$$

The evolution equations of the antiparticles are obtained by taking the CP conjugates of the different rates. The Boltzmann equations of the number density (asymmetry) finally read:

$$Y'_{N_3} \;=\; (1-y_{N_3})\left(\gamma_D + 2\sum_{k=a,\ldots,e}\gamma^k_{N_3}\right) , \tag{C1}$$

$$\begin{aligned} Y'_{\Delta N_D} \;=\;& (y_{N_3}-1)\left(\epsilon_{CP}\,\gamma_D + 2\,\epsilon^a_{CP}\,\gamma^a_{N_3} - 2\,\epsilon^b_{CP}\,\gamma^b_{N_3} - 2\,\epsilon^c_{CP}\,\gamma^c_{N_3}\right) \\ &-\; 2\left(\gamma^a_{\Delta\,2} + 2\gamma^b_{\Delta\,2}\right)(y_{\Delta N_D} - y_{\Delta S}) - \gamma^a_{N_3}\,(y_{N_3}y_{\Delta N_D} - y_{\Delta H_3} + y_{\Delta S}) \\ &-\; \gamma^b_{N_3}\,(y_{\Delta N_D} - y_{\Delta H_3} + y_{N_3}y_{\Delta S}) - \gamma^c_{N_3}\,(y_{\Delta N_D} - y_{N_3}y_{\Delta H_3} + y_{\Delta S}) \\ &-\; \gamma_{D\ell}\,(y_{\Delta N_D} - y_{\Delta\ell} - y_{\Delta H_1}) - \gamma_{D\bar{\ell}}\,(y_{\Delta N_D} + y_{\Delta\ell} + y_{\Delta H_2}) \\ &-\; \left(\gamma^s_{N_D} + 2\gamma^t_{N_3}\right)(y_{\Delta N_D} - y_{\Delta\ell}) , \end{aligned} \tag{C2}$$

$$\begin{aligned} Y'_{\Delta S} \;=\;& -(y_{N_3}-1)\left(\epsilon_{CP}\,\gamma_D + 2\,\epsilon^a_{CP}\,\gamma^a_{N_3} - 2\,\epsilon^b_{CP}\,\gamma^b_{N_3} - 2\,\epsilon^c_{CP}\,\gamma^c_{N_3} + 2\,\epsilon_{CP}\,\gamma^d_{N_3} + 2\,\epsilon_{CP}\,\gamma^e_{N_3}\right) \\ &-\; 2\left(\gamma^a_{\Delta\,2} + 2\gamma^b_{\Delta\,2}\right)(y_{\Delta S} - y_{\Delta N_D}) \;-\; 2\gamma_{SS}\,(2y_{\Delta S} - y_{\Delta H_1} + y_{\Delta H_2}) \\ &-\; \gamma^a_{N_3}\,(y_{\Delta S} - y_{\Delta H_3} + y_{N_3}y_{\Delta N_D}) - \gamma^b_{N_3}\,(y_{N_3}y_{\Delta S} - y_{\Delta H_3} + y_{\Delta N_D}) \\ &-\; \gamma^c_{N_3}\,(y_{\Delta S} - y_{N_3}y_{\Delta H_3} + y_{\Delta N_D}) - \gamma^d_{N_3}\,(y_{N_3}y_{\Delta S} - y_{\Delta H_1} - y_{\Delta\ell}) \\ &-\; \gamma^e_{N_3}\,(y_{N_3}y_{\Delta S} + y_{\Delta H_2} + y_{\Delta\ell}) , \end{aligned} \tag{C3}$$

$$\begin{aligned} Y'_{\Delta\ell} \;=\;& -(y_{N_3}-1)\left(2\,\epsilon_{CP}\,\gamma^d_{N_3} - 2\,\epsilon_{CP}\,\gamma^e_{N_3}\right) - \gamma_{D\,\ell}\,(y_{\Delta\ell} + y_{\Delta H_1} - y_{\Delta N_D}) \\ &-\; \gamma_{D\,\bar{\ell}}\,(y_{\Delta\ell} + y_{\Delta H_2} + y_{\Delta N_D}) + \left(\gamma^s_{N_D} + 2\gamma^t_{N_3}\right)(y_{\Delta N_D} - y_{\Delta\ell}) - \left(\gamma^a_{\ell\ell} + 2\,\gamma^b_{\ell\ell}\right)(2y_{\Delta\ell} + y_{\Delta H_1} + y_{\Delta H_2}) \\ &-\; \gamma^d_{N_3}\,(y_{\Delta H_1} + y_{\Delta\ell} - y_{N_3}y_{\Delta S}) - \gamma^e_{N_3}\,(y_{\Delta H_2} + y_{\Delta\ell} + y_{N_3}y_{\Delta S}) , \end{aligned} \tag{C4}$$

$$\begin{aligned} Y'_{\Delta H_1} \;=\;& -2\,(y_{N_3}-1)\,\epsilon_{CP}\,\gamma^d_{N_3} - \gamma_{D\,\ell}\,(y_{\Delta H_1} + y_{\Delta\ell} - y_{\Delta N_D}) - \left(\gamma^a_{\ell\ell} + \gamma^b_{\ell\ell}\right)(2y_{\Delta\ell} + y_{\Delta H_1} + y_{\Delta H_2}) \\ &-\; \gamma^d_{N_3}\,(y_{\Delta H_1} + y_{\Delta\ell} - y_{N_3}y_{\Delta S}) - \gamma_{SS}\,(y_{\Delta H_1} - y_{\Delta H_2} - 2\,y_{\Delta S}) , \end{aligned} \tag{C5}$$

$$\begin{aligned} Y'_{\Delta H_2} \;=\;& 2\,(y_{N_3}-1)\,\epsilon_{CP}\,\gamma^e_{N_3} - \gamma_{D\,\bar{\ell}}\,(y_{\Delta H_2} + y_{\Delta\ell} + y_{\Delta N_D}) - \left(\gamma^a_{\ell\ell} + \gamma^b_{\ell\ell}\right)(2y_{\Delta\ell} + y_{\Delta H_1} + y_{\Delta H_2}) \\ &-\; \gamma^e_{N_3}\,(y_{\Delta H_2} + y_{\Delta\ell} + y_{\Delta S}\,y_{N_3})\,\gamma_{SS}\,(y_{\Delta H_2} - y_{\Delta H_1} + 2\,y_{\Delta S}) , \end{aligned} \tag{C6}$$

$$\begin{aligned} Y'_{\Delta H_3} \;=\;& (y_{N_3}-1)\left(2\,\epsilon^a_{CP}\,\gamma^a_{N_3} - 2\,\epsilon^b_{CP}\,\gamma^b_{N_3} - 2\,\epsilon^c_{CP}\,\gamma^c_{N_3}\right) - \gamma^a_{N_3}\,(y_{\Delta H_3} - y_{\Delta S} - y_{\Delta N_D}y_{N_3}) \\ &-\; \gamma^b_{N_3}\,(y_{\Delta H_3} - y_{\Delta N_D} - y_{\Delta S}y_{N_3}) - \gamma^c_{N_3}\,(y_{\Delta H_3}y_{N_3} - y_{\Delta N_D} - y_{\Delta S}) . \end{aligned} \tag{C7}$$

Appendix D: Chemical Equilibrium Conditions

	c_{B-L}	c_{N_D}	c_S	c_{B-L}	c_{N_D}	c_{B-L}
μ_{H_1}	$\frac{1}{16}$	$\frac{15}{16}$	0	$\frac{1}{16}$	$\frac{15}{16}$	$-\frac{1}{14}$
μ_{H_2}	$-\frac{11}{16}$	$-\frac{101}{16}$	0	$-\frac{11}{16}$	$-\frac{101}{16}$	$\frac{3}{14}$
μ_{H_3}	$-\frac{9}{8}$	$-\frac{101}{8}$	$-\frac{1}{2}$	$-\frac{21}{16}$	$-\frac{231}{16}$	$\frac{3}{4}$
μ_S	0	0	1	$\frac{3}{8}$	$\frac{29}{8}$	$-\frac{1}{7}$
μ_{N_D}	0	1	0	0	1	$-\frac{1}{7}$
μ_ℓ	$-\frac{1}{16}$	$\frac{1}{16}$	0	$-\frac{1}{16}$	$\frac{1}{16}$	$-\frac{1}{14}$

TABLE II: Chemical equilibrium coefficients in eq. (D12) for the three cases discussed in the text.

We derive in this section the chemical equilibrium conditions provided by all the interactions which are in equilibrium at the leptogenesis epoch, $T \sim M_3 \lesssim 10^{5\div 6}\,\mathrm{GeV}$.

The chemical potentials of each generation of $SU(2)_W$ quark doublets, Q_i, and singlets, u_{Ri} and d_{Ri}, are denoted by $\mu_{Q_i} \equiv \mu_Q$, $\mu_{u_{Ri}} \equiv \mu_u$ and $\mu_{d_{Ri}} \equiv \mu_d$, respectively. Concerning the lepton fields, we define for each flavor α the corresponding chemical potentials as: $\mu_{\ell_\alpha} \equiv \mu_\ell$, $\mu_{e_{R\alpha}} \equiv \mu_e$. We denote with μ_N the chemical potential of N_D. Analogously, for each scalar field in the model we define, in a consistent notation: $\mu_{H_{1,2,3}}$ and μ_S. We remark that the chemical potentials of the SM fermions are assumed to be independent of the generation index, because of the the rapid flavor mixing interactions which occur at the leptogenesis time [42].

The number density asymmetries are related to the particle chemical potentials through the relations:

$$Y_{\Delta X} \simeq \frac{g_X\, T^3}{3s}\,\mu_X \quad \text{for bosons}\,, \tag{D1}$$

$$Y_{\Delta X} \simeq \frac{g_X\, T^3}{6s}\,\mu_X \quad \text{for fermions}\,, \tag{D2}$$

where g_X is the number of internal degrees of freedom of the particle X. The total baryon and lepton number asymmetries can be expressed in terms of the fermion chemical potentials:

$$Y_{\Delta B} = \frac{T^3}{2s}\left(2\mu_Q + \mu_u + \mu_d\right)\,, \quad Y_{\Delta L} = \frac{T^3}{2s}\left(2\mu_\ell + \mu_e + \frac{2}{3}\mu_{N_D}\right)\,. \tag{D3}$$

Taking into account the definitions given above, we have the following relations [42]:

1. QCD and $SU(2)_W$ sphaleron interactions:

$$2\mu_Q - \mu_u - \mu_d = 0\,, \tag{D4}$$
$$3\mu_Q + \mu_\ell = 0\,. \tag{D5}$$

2. Hypercharge neutrality:

$$3\left(\mu_Q + 2\mu_u - \mu_d - \mu_\ell - \mu_e\right) + 2\left(\mu_{H_1} + \mu_{H_2}\right) = 0\,. \tag{D6}$$

3. Charged lepton Yukawa interactions:

$$\mu_\ell - \mu_{H_1} - \mu_e = 0\,, \tag{D7}$$
$$\mu_Q + \mu_{H_1} - \mu_u = 0\,, \tag{D8}$$
$$\mu_Q - \mu_{H_1} - \mu_d = 0\,. \tag{D9}$$

4. Lepton number conserving Dirac neutrino Yukawa interactions:

$$\mu_{N_D} - \mu_{H_1} - \mu_\ell = 0\,. \tag{D10}$$

5. $(B - \widetilde{L})$ conservation:

$$3\,\left(2\mu_Q + \mu_u + \mu_d\right) - 3\left(2\mu_\ell + \mu_e\right) - 2\mu_{N_D} - 2\left(\mu_S + 2\mu_{H_3} - 4\mu_{H_2}\right) = 0\,. \tag{D11}$$

We notice that the QCD sphaleron condition is redundant in this case, as all quark Yukawa interactions are in equilibrium.

The different chemical equilibrium conditions enforce relations among the chemical potentials, which then can be expressed in terms of a subset of them. We set

$$\mu_X \;=\; c_{B-L}\,\mu_{B-L} \,+\, c_{N_D}\,\mu_{N_D} \,+\, c_S\,\mu_S\,, \tag{D12}$$

where we define μ_{B-L} through the relation: $Y_{\Delta(B-L)} \equiv Y_{\Delta B} - Y_{\Delta L} \equiv \mu_{B-L}\, T^3/(2s)$. We then distinguish three possible scenarios:

A. Lepton number violating neutrino Yukawa interactions and S self-annihilation are decoupled, which corresponds to the set of equilibrium conditions $1-5$ listed above. The different chemical potentials can be expressed in terms of the set $(\mu_{B-L}, \mu_{N_D}, \mu_S)$.

B. S self annihilations are always in equilibrium, but lepton number violating Yukawa interactions are still decoupled. An additional equilibrium condition is enforced:

$$2\mu_S - \mu_{H_1} + \mu_{H_2} = 0\,. \tag{D13}$$

Only two chemical potentials are independent, that we choose to be (μ_{B-L}, μ_{N_D}).

C. All interactions listed above, as well as lepton number violating Yukawa interactions, are in thermal equilibrium during the leptogenesis era:

$$\mu_{N_D} + \mu_{H_2} + \mu_\ell = 0\,. \tag{D14}$$

In this case, all chemical potentials are proportional and can be expressed for example in terms of μ_{B-L}.

The coefficients c_X in eq. (D12), corresponding to the three cases listed above are reported in Tab. D. In the first two cases the final baryon asymmetry is given by

$$Y_{\Delta B} \;=\; \frac{1}{4}\, Y_{\Delta(B-L)} - \frac{1}{8}\, Y_{\Delta N_D}\,. \tag{D15}$$

In the last scenario, which corresponds to the case discussed in Section III, where all the interactions listed above are in thermal equilibrium during the generation of the BAU, we have:

$$Y_{\Delta B} \;=\; \frac{2}{7}\, Y_{\Delta(B-L)}\,. \tag{D16}$$

Notice that expressions (D15) and (D16) should be considered valid up to the decoupling of N_D, *i.e.* for $\Gamma_{N_D} \gg H$.

[1] B. T. Cleveland *et al.*, Astrophys. J. **496**, 505 (1998).
[2] Y. Fukuda *et al.* [Kamiokande Collaboration], Phys. Rev. Lett. **77** (1996) 1683.
[3] P. Anselmann *et al.* [GALLEX Collaboration], Phys. Lett. B **285** (1992) 390; W. Hampel *et al.*, Phys. Lett. B **447** (1999) 127.
[4] M. Altmann *et al.* [GNO COLLABORATION Collaboration], Phys. Lett. B **616** (2005) 174 [arXiv:hep-ex/0504037].
[5] S. Fukuda *et al.* [Super-Kamiokande Collaboration], Phys. Lett. B **539**, 179 (2002) [arXiv:hep-ex/0205075]; Y. Fukuda *et al.*, Phys. Rev. Lett. **81**, 1562 (1998) [arXiv:hep-ex/9807003]; Y. Ashie *et al.*, Phys. Rev. Lett. **93** (2004) 101801.
[6] Q. R. Ahmad *et al.* [SNO Collaboration], Phys. Rev. Lett. **87**, 071301 (2001) [arXiv:nucl-ex/0106015].
[7] K. Eguchi *et al.* [KamLAND Collaboration], Phys. Rev. Lett. **90** (2003) 021802; T. Araki *et al.*, Phys. Rev. Lett. **94** (2005) 081801.
[8] C. Arpesella *et al.* [Borexino Collaboration], Phys. Lett. B **658**, 101 (2008) [arXiv:0708.2251 [astro-ph]]; Phys. Rev. Lett. **101**, 091302 (2008) [arXiv:0805.3843 [astro-ph]].
[9] M. H. Ahn *et al.* [K2K Collaboration], Phys. Rev. D **74** (2006) 072003.
[10] D. G. Michael *et al.* [MINOS Collaboration], Phys. Rev. Lett. **97**, 191801 (2006) [arXiv:hep-ex/0607088]; P. Adamson *et al.*, Phys. Rev. Lett. **101**, 221804 (2008) [arXiv:0807.2424 [hep-ex]].
[11] K. Nakamura *et at.* (Particle Data Group), J. Phys. G **37** (2010) 075021.
[12] B. Pontecorvo, Zh. Eksp. Teor. Fiz. (JETP) **33** (1957) 549 and **34** (1958) 247.
[13] Z. Maki, M. Nakagawa and S. Sakata, Prog. Theor. Phys. **28** (1962) 870.
[14] B. Pontecorvo, Sov. Phys. JETP **26** (1968) 984. [Zh. Eksp. Teor. Fiz. **53**, 1717 (1967)].
[15] K. Abe *et al.* [T2K Collaboration], Phys. Rev. Lett. **107**, 041801 (2011) [arXiv:1106.2822 [hep-ex]].
[16] E. Komatsu *et al.* [WMAP Collaboration], Astrophys. J. Suppl. **192** (2011) 18 [arXiv:1001.4538 [astro-ph.CO]].
[17] G. Bertone, D. Hooper, J. Silk, Phys. Rept. **405** (2005) 279-390. [hep-ph/0404175]; L. Bergstrom, New J. Phys. **11** (2009) 105006. [arXiv:0903.4849 [hep-ph]]; J. L. Feng, Ann. Rev. Astron. Astrophys. **48**, 495 (2010). [arXiv:1003.0904 [astro-ph.CO]].
[18] Z. Ahmed *et al.* [The CDMS-II Collaboration], Science **327** (2010) 1619 [arXiv:0912.3592 [astro-ph.CO]].
[19] R. Bernabei *et al.*, Eur. Phys. J. C **67** (2010) 39 [arXiv:1002.1028 [astro-ph.GA]].
[20] C. E. Aalseth *et al.* [CoGeNT collaboration], Phys. Rev. Lett. **106** (2011) 131301 [arXiv:1002.4703 [astro-ph.CO]].
[21] E. Aprile *et al.* [XENON100 Collaboration], arXiv:1104.2549 [astro-ph.CO].
[22] B.D. Fields and S. Sarkar, in the review of BBN in [11].
[23] M. Fukugita and T. Yanagida, Phys. Lett. B **174** (1986) 45.
[24] M. A. Luty, Phys. Rev. D **45**, 455 (1992).

[25] Type I seesaw: P. Minkowski, Phys. Lett. B **67** (1977) 421; M. Gell-Mann, P. Ramond and R. Slansky, Proceedings of the Supergravity Stony Brook Workshop, New York 1979, eds. P. Van Nieuwenhuizen and D. Freedman; T. Yanagida, Proceedinds of the Workshop on Unified Theories and Baryon Number in theUniverse, Tsukuba, Japan 1979, ed.s A. Sawada and A. Sugamoto; R. N. Mohapatra and G. Senjanovic, Phys. Rev. Lett. **44** (1980) 912.
Type II seesaw: W. Konetschny, W. Kummer, Phys. Lett. **B70** (1977) 433; T. P. Cheng, L. -F. Li, Phys. Rev. **D22**, 2860 (1980); G. Lazarides, Q. Shafi, C. Wetterich, Nucl. Phys. **B181**, 287 (1981); J. Schechter, J. W. F. Valle, Phys. Rev. **D22**, 2227 (1980); R. N. Mohapatra, G. Senjanovic, Phys. Rev. **D23**, 165 (1981).

[26] S. Gabriel and S. Nandi, Phys. Lett. B **655** (2007) 141 [arXiv:hep-ph/0610253]; A. Pilaftsis, Phys. Rev. **D78**, 013008 (2008). [arXiv:0805.1677 [hep-ph]]; M. Aoki, S. Kanemura, O. Seto, Phys. Rev. Lett. **102**, 051805 (2009). [arXiv:0807.0361 [hep-ph]]; F. Bazzocchi, Phys. Rev. D **83**, 093009 (2011) [arXiv:1011.6299 [hep-ph]]; N. Haba and K. Tsumura, JHEP **1106** (2011) 068 [arXiv:1105.1409 [hep-ph]]; M. Lindner, D. Schmidt and T. Schwetz, arXiv:1105.4626 [hep-ph].

[27] R. N. Mohapatra and J. W. F. Valle, Phys. Rev. D **34** (1986) 1642.

[28] V. A. Kuzmin, V. A. Rubakov and M. E. Shaposhnikov, Phys. Lett. B **155** (1985) 36.

[29] L. Wolfenstein, Nucl. Phys. B **186** (1981) 147.

[30] S. T. Petcov, Phys. Lett. B **110** (1982) 245.

[31] G. C. Branco, W. Grimus and L. Lavoura, Nucl. Phys. B **312**, 492 (1989).

[32] F. del Aguila, J. A. Aguilar-Saavedra and R. Pittau, J. Phys. Conf. Ser. **53**, 506 (2006) [arXiv:hep-ph/0606198]; F. del Aguila, J. A. Aguilar-Saavedra, Phys. Lett. **B672**, 158-165 (2009). [arXiv:0809.2096 [hep-ph]].

[33] A. Ibarra, E. Molinaro and S. T. Petcov, JHEP **1009**, 108 (2010) [arXiv:1007.2378 [hep-ph]]; A. Ibarra, E. Molinaro and S. T. Petcov, Phys. Rev. D **84**, (2011) 013005 [arXiv:1103.6217 [hep-ph]].

[34] M. B. Gavela, T. Hambye, D. Hernandez and P. Hernandez, JHEP **0909** (2009) 038 [arXiv:0906.1461 [hep-ph]].

[35] S. Davidson, E. Nardi and Y. Nir, Phys. Rept. **466** (2008) 105 [arXiv:0802.2962 [hep-ph]].

[36] L. Bento, JCAP **0311**, 002 (2003) [arXiv:hep-ph/0304263].

[37] J. Liu, G. Segre, Phys. Rev. **D48**, 4609-4612 (1993). [hep-ph/9304241]; L. Covi, E. Roulet, F. Vissani, Phys. Lett. **B384**, 169-174 (1996). [hep-ph/9605319].

[38] T. Hahn, Comput. Phys. Commun. **140** (2001) 418 [arXiv:hep-ph/0012260]. http://www.feynarts.de

[39] T. Hahn, PoS A **CAT08** (2008) 121 [arXiv:0901.1528 [hep-ph]].

[40] N. D. Christensen and C. Duhr, Comput. Phys. Commun. **180** (2009) 1614 [arXiv:0806.4194 [hep-ph]].

[41] W. Buchmuller, P. Di Bari and M. Plumacher, Annals Phys. **315** (2005) 305 [arXiv:hep-ph/0401240].

[42] J. A. Harvey and M. S. Turner, Phys. Rev. D **42** (1990) 3344.; M. Laine and M. E. Shaposhnikov, Phys. Rev. D **61** (2000) 117302 [arXiv:hep-ph/9911473].

[43] C. S. Fong, M. C. Gonzalez-Garcia, J. Racker, Phys. Lett. **B697**, 463-470 (2011). [arXiv:1010.2209 [hep-ph]].

[44] G. F. Giudice, A. Notari, M. Raidal, A. Riotto and A. Strumia, Nucl. Phys. B **685**, 89 (2004) [arXiv:hep-ph/0310123].

[45] A. Pilaftsis and T. E. J. Underwood, Phys. Rev. D **72** (2005) 113001 [arXiv:hep-ph/0506107].

[46] Y. Chikashige, R. N. Mohapatra and R. D. Peccei, Phys. Lett. B **98** (1981) 265; J. Schechter, J. W. F. Valle, Phys. Rev. **D25**, 774 (1982).

[47] E. Ma, Phys. Rev. Lett. **86** (2001) 2502 [arXiv:hep-ph/0011121].

[48] W. Grimus, L. Lavoura and B. Radovcic, Phys. Lett. B **674** (2009) 117 [arXiv:0902.2325 [hep-ph]].

[49] G. 't Hooft, NATO Adv. Study Inst. Ser. B Phys. **59** (1980) 135.

[50] S. B. Giddings and A. Strominger, Nucl. Phys. B **307** (1988) 854.

[51] E. K. Akhmedov, Z. G. Berezhiani, R. N. Mohapatra and G. Senjanovic, Phys. Lett. B **299** (1993) 90 [arXiv:hep-ph/9209285].

[52] D. S. P. Dearborn, D. N. Schramm and G. Steigman, Phys. Rev. Lett. **56** (1986) 26; H. Y. Cheng, Phys. Rev. D **36** (1987) 1649; R. Chanda, J. F. Nieves and P. B. Pal, Phys. Rev. D **37** (1988) 2714; K. Choi and A. Santamaria, Phys. Rev. D **42** (1990) 293; A. Pilaftsis, Phys. Rev. D **49** (1994) 2398 [arXiv:hep-ph/9308258]; Y. Farzan, Phys. Rev. **D67**, 073015 (2003). [hep-ph/0211375].

[53] [LEP Higgs Working Group for Higgs boson searches and ALEPH Collaboration], arXiv:hep-ex/0107031.

[54] R. Barate *et al.* [LEP Working Group for Higgs boson searches and ALEPH Collaboration and and], Phys. Lett. B **565** (2003) 61 [arXiv:hep-ex/0306033].

[55] A. Djouadi, Phys. Rept. **457** (2008) 1 [arXiv:hep-ph/0503172].

[56] G. Belanger, F. Boudjema, A. Pukhov and A. Semenov, arXiv:1005.4133 [hep-ph]. G. Belanger, F. Boudjema, A. Pukhov and A. Semenov, arXiv:0803.2360 [hep-ph]. G. Belanger, F. Boudjema, A. Pukhov and A. Semenov, Comput. Phys. Commun. **176** (2007) 367 [arXiv:hep-ph/0607059].

[57] V. Silveira, A. Zee, Phys. Lett. **B161**, 136 (1985); J. McDonald, Phys. Rev. D **50** (1994) 3637 [arXiv:hep-ph/0702143]; C. P. Burgess, M. Pospelov and T. ter Veldhuis, Nucl. Phys. B **619**, 709 (2001) [arXiv:hep-ph/0011335]; V. Barger, P. Langacker, M. McCaskey, M. J. Ramsey-Musolf and G. Shaughnessy, Phys. Rev. D **77** (2008) 035005 [arXiv:0706.4311 [hep-ph]]. M. Farina, D. Pappadopulo and A. Strumia, Phys. Lett. B **688**, 329 (2010) [arXiv:0912.5038 [hep-ph]]; W. L. Guo and Y. L. Wu, JHEP **1010**, 083 (2010) [arXiv:1006.2518 [hep-ph]].

[58] B. Patt and F. Wilczek, arXiv:hep-ph/0605188; J. March-Russell, S. M. West, D. Cumberbatch and D. Hooper, JHEP **0807** (2008) 058 [arXiv:0801.3440 [hep-ph]].

[59] J. Gasser, H. Leutwyler and M. E. Sainio, Phys. Lett. B **253** (1991) 260.

[60] C. Arina, F. X. Josse-Michaux and N. Sahu, Phys. Rev. D **82** (2010) 015005 [arXiv:1004.3953 [hep-ph]].

[61] Cf. talk of T. Marrodán Undagoitia "Mini-review Direct Dark Matter Detection and recent XENON100 results" at HEP-EPS-2011, Grenoble.

[62] A. Abada, S. Davidson, A. Ibarra, F. X. Josse-Michaux, M. Losada and A. Riotto, JHEP **0609** (2006) 010 [arXiv:hep-ph/0605281].
[63] E. Nardi, J. Racker, E. Roulet, JHEP **0709**, 090 (2007). [arXiv:0707.0378 [hep-ph]].